



Elemental composition of atmospheric PM₁₀ during COVID-19 lockdown and recovery periods in Moscow (April–July 2020)

Anastasia D. Serdyukova · Dmitrii V. Vlasov ·
Olga B. Popovicheva · Natalia E. Kosheleva ·
Marina A. Chichayeva · Nikolay S. Kasimov

Received: 29 May 2023 / Accepted: 17 July 2023 / Published online: 27 July 2023
© The Author(s), under exclusive licence to Springer Nature B.V. 2023

Abstract Changes in the concentrations of PM₁₀-bound potentially toxic elements (PTEs) during the COVID-19 lockdown period and after the revocation of restrictions were analyzed using the data received at the Aerosol Complex of Moscow State University in April–July 2020. During the lockdown, the input of biomass combustion products enriched in PTEs from the Moscow region hindered the decrease in pollutant concentrations. After the introduction of the self-isolation regime, lower concentrations of most PTEs occurred due to the decrease in anthropogenic activity and the rainy meteorological conditions. After the revocation of restrictive measures, the PTE concentrations began to increase. Multivariate statistical analysis (APCA-MLR) identified

the main sources of atmospheric pollutants as urban dust, non-exhaust traffic emissions, and combustion and exhaust traffic emissions. PM₁₀ particles were significantly enriched with Sb, Cd, Sn, Bi, S, Pb, Cu, Mo, and Zn. The total non-carcinogenic and carcinogenic risks, calculated according to the U.S. EPA model, decreased by 24% and 23% during the lockdown; after the removal of restrictions, they increased by 61% and 72%, respectively. The study provides insight into the PTE concentrations and their main sources at different levels of anthropogenic impact.

Keywords Lockdown · Health risk · Traffic · Urban dust · Potentially toxic elements · Source identification

Supplementary Information The online version contains supplementary material available at <https://doi.org/10.1007/s10653-023-01698-2>.

A. D. Serdyukova · D. V. Vlasov (✉) · N. E. Kosheleva ·
M. A. Chichayeva · N. S. Kasimov
Faculty of Geography, Lomonosov Moscow State
University, Moscow 119991, Russian Federation
e-mail: vlasov.msu@gmail.com

D. V. Vlasov
Department of Geography, Geology, and the Environment,
Illinois State University, Normal, IL 61790, USA

O. B. Popovicheva
Skobeltsyn Institute of Nuclear Physics, Lomonosov
Moscow State University, Moscow 119991,
Russian Federation

Introduction

Atmospheric pollution with particulate matter (PM) is among the main problems for the population in large cities, leading to higher cardiopulmonary mortality, respiratory diseases (asthma, bronchitis, rhinitis, etc.), increased hospitalizations (WHO, 2013), and global reduction in life expectancy by 2 years (Greenstone & Fan, 2018). Potentially toxic elements (PTEs) are the primary determinant of biological reactions caused by exposure of organisms to particles with a diameter of 10 μm or less (PM₁₀). Among them, Cd, Pb, As, Hg, Ni, Cr, Cu, Zn, and Sb are particularly dangerous (Pourret & Hursthouse, 2019; Van Den Heuvel

et al., 2016). PTEs could cause respiratory symptoms, decreased lung function, asthma (Ali et al., 2019), DNA oxidation and damage, and provoke cardiovascular and neurodegenerative diseases and various types of cancer (Ghanbarian et al., 2019).

The period of restrictive measures introduced in many cities worldwide to reduce the incidence of a novel coronavirus infection COVID-19 has led to the most significant decrease in human endeavor in recent decades due to a major setback in business, industrial, and transport activities. As a result, lower anthropogenic emissions caused a reduction in concentrations of many gaseous compounds, PM, and other pollutants (Hartwell et al., 2021; He et al., 2021; Huang et al., 2023; Hudda et al., 2020; Lara et al., 2023; Sokhi et al., 2021). This, in turn, reduces public health risks posed by air pollution. For instance, reducing PM_{10} atmospheric concentrations by only 7.65% allowed the avoidance of an average of 10,000 additional deaths of the population from polluted air in 352 cities in China in 2020 (Qiu et al., 2021). Thus, the lockdowns provided a unique opportunity to undertake a real-time experiment and monitor the relationship between emission sources and aerosol chemistry under rapidly changing anthropogenic pressure (Jia et al., 2021).

The relationship between air pollution with PTEs and the introduction of restrictive measures has been studied to a lesser extent, although the relative contribution of chemical elements to the total mass of aerosols may increase during the lockdown due to a sharp decrease in other components, e.g., water-soluble ions, black carbon and secondary inorganic aerosols (Manchanda et al., 2021). For instance, in Elche, Spain, due to a 35–80% decrease in the transport load, the concentrations of K, Ni, Cu, Mn, Zn, Ca, and Fe in PM_{10} decreased up to 80% (Clemente et al., 2022). The same effect was observed in Andalusia during the lockdown when concentrations of PM_{10} -bound Sb and Sn decreased by 30–40%. The concentrations of many other PTEs have declined due to local factors unrelated to the pandemic, such as the shift of industries to new fuels or raw materials (Millán-Martínez et al., 2022). On the other hand, despite a decrease in the concentrations of Pb, Zn, Cu, K, Cd, Se, Ba, Ca, As, Sr, Al, Mn, and Mg in $PM_{2.5}$ by 20–53% due to the lesser influence of motor transport, construction, and dust blowing during the partial lockdown

in Hanoi, Vietnam, an increase in the concentrations of Ni, Co, Mo, and Cr by 38–90% was observed as a result of the ongoing activity of industrial enterprises and unfavorable meteorological conditions for the dispersion of pollutants (Nguyen et al., 2021). Moreover, a significant reduction in air pollution with PM_{10} compared to $PM_{2.5}$ during the lockdown resulted from decreasing non-exhaust transport emissions (road dust blowing and wear of car parts) and construction/demolition dust (Querol et al., 2021). As a result, lower contamination of aerosols with PTEs, especially Cr, Ni, Cd, As, Pb, Zn, Co, Cu, V, and Mn, during the restrictive measures and even haze episodes has reduced non-carcinogenic and carcinogenic risks for the population (Wang et al., 2021b, d).

As in many cities worldwide, restrictive measures were introduced in Moscow to combat the spread of COVID-19. During the lockdown, PM_{10} air pollution decreased by 28% compared to the long-term average, mainly due to a fourfold reduction in road traffic (Ginzburg et al., 2020). The lower air pollution was supported by meteorological conditions such as increased temperatures in the cold winter-spring period compared to the interannual average for this period, as well as low temperatures and heavy precipitation in some episodes during the lockdown (Chubarova et al., 2021). At the same time, the impact of the lockdown on the precipitation composition was ambivalent: purification of the atmosphere from aerosols during their long-term washing out by precipitation and a decrease in anthropogenic emissions caused the decrease in the precipitation pollution with PTEs by 10–99% while air advection to Moscow from the suburbs, where wood, coal, household and agricultural wastes were burned contributed to the growth of precipitation pollution with P, Ag, Pb, Cd, Sb, As (Vlasov et al., 2023a). The contribution of biomass burning in the residential areas in the suburbs to the black carbon concentrations in Moscow aerosols also increased during the lockdown (Popovicheva et al., 2022).

The enrichment of PM_{10} with PTEs during the May holidays in the lockdown period was studied in the center of Moscow (Gubanova et al., 2021b). An increase in concentrations of many PTEs, especially P, Pb, Al, S, Ni, Sn, Sb, Bi, Se, and Th, in PM_{10} was observed compared to April. However, the lack of data on PTE levels after the lockdown in this study

has not made it possible to assess the impact of restrictions on air pollution. There are no data on PTEs in urban background conditions, making it difficult to assess the overall level of their content in the urban air. Detailed assessments of PM_{10} emissions from various sources have been carried out, the long-term dynamics of PM_{10} concentrations in different parts of the city have been studied (Elansky et al., 2018), and weekly patterns and weekend effects of air pollution have been identified in Moscow (Elansky et al., 2020). However, the content of PTEs in atmospheric PM_{10} has only been analyzed for the central part of the city in certain seasons (Gubanova et al., 2021a, b) and under the influence of local sources (Gubanova et al., 2022). There are practically no data on the level of PTEs in the urban background conditions, which makes it impossible to understand the ratio of various urban and suburban sources that affect the levels and variability of PTE concentrations in the megacity air.

For this reason, the study aims to analyze changes in PM_{10} -bound PTEs concentrations during and after the lifting of restrictions in Moscow urban background. Specific tasks include considering the influence of anthropogenic sources and precipitation on the chemical composition of atmospheric PM_{10} ; quantitatively assessing the contributions of PTE sources during and after the lockdown period; and calculating the total non-carcinogenic and carcinogenic risks for the population during the lockdown period and after the lifting of restrictive measures.

Materials and methods

Study area and sampling

Moscow is situated within the European territory of Russia, covering an area of 2561 km² with a population of over 12.66 million people. The main source of anthropogenic environmental impact is motor transport: in 2019, gaseous emissions from motor vehicles amounted to 345,000 tons, accounting for 85% of the total emissions into the atmosphere (Kul'bachevskii, 2020). In 2020, emissions decreased by 5400 tons compared to 2019, partly due to the implementation of restrictive measures (Kul'bachevskii, 2021). Roads occupy approximately 8% of the city's area,

and by the end of 2019, the total length of roads was 6625 km (Russian Federal State Statistics Service, 2020). There are more than 3000 industrial enterprises in Moscow, which occupy 17% of the city's area. Thermal power plants (TPPs) primarily use natural gas as fuel (99.5% of the total) contributing 50–65% of industrial gaseous emissions released into the atmosphere. Oil refineries account for a significant contribution of 20–30%, while other industries contribute 15–20% (Bityukova & Saulskaya, 2017). An increase in the PM_{10} concentrations in the atmosphere of Moscow is often associated with unfavorable meteorological conditions (Kul'bachevskii, 2021). Additional air pollution arises from suburban areas where many industrial enterprises and summer cottages are located, and residents burn biomass and garbage for recycling and heating purposes (Popovich et al., 2022; Vlasov et al., 2023a). In spring and summer, barbecues serve as a significant source of pollutants, primarily found in city parks and country homesteads.

Sampling was conducted at the Aerosol complex of MSU (55.707°N, 37.522°E), situated within the premises of the Metrological Observatory of Lomonosov Moscow State University (MO MSU). MO MSU is located far from industrial sources and major highways (Fig. 1); it serves as an urban background station (Chubarova et al., 2014).

The self-isolation regime to combat the spread of COVID-19 in Moscow was implemented on March 30, 2020. Starting from June 1, car dealerships, non-food stores, weekend fairs, and some consumer service enterprises resumed their operations. Access control and self-isolation measures were lifted on June 9 (Measures against coronavirus in Moscow, 2020). Throughout the lockdown period, the average traffic congestion level in Moscow did not exceed 20% according to the TomTom index (Fig. 2). During the recovery period, it increased to 40–45% on weekends and 36–72% on weekdays (TomTom Traffic Index, 2020). The number of cars on the roads during the weekdays decreased by approximately 40% during the lockdown, and pre-pandemic levels were only reached by mid-June (Kirilina, 2020). The Yandex self-isolation index (YSII) measures the city activity level compared to a typical day before the pandemic (Fig. S1) and confirms a significant



Fig. 1 Location of the Aerosol complex of MSU in the southwestern sector of Moscow

decrease in transport activity during the period of restrictions (Yandex, 2021).

PM₁₀ samples were collected at 24-h intervals, starting from 5 p.m. on a given day and continuing until 5 p.m. the next day. The sampling process involved using 47 mm polyethylene terephthalate filters and a PM₁₀ impactor, with an airflow rate of 16 L/min. The total volume of air pumped was considered under standard atmospheric conditions. Based on the YSII and TomTom indices, dates of restrictions implementation and removal, as well as considering the timing of the heating season in Moscow, the PM₁₀ sampling periods were categorized as follows: lockdown period 1 (L1) occurred during the heating season with restrictive measures (April 24–May 11, 13 samples); lockdown period 2 (L2) began after the heating season ended (May 12–May 31; 16 samples), recovery period 1 (R1) aligned with the initial phase of restrictions easing (June 1–June 14; 7 samples); recovery period 2 (R2) encompassed the gradual resumption of activities (June 15–July 30; 33 samples). During June and the first half of July, samples were collected every other day, while daily sampling was conducted during other periods. Thus, a total of 69 samples were collected. PM₁₀ mass concentrations were measured by the Mosecomonitoring institution using the tampered element oscillating microbalance TEOM 1400a (Thermo Environmental Instruments Inc., USA).

Meteorological conditions

Meteorological conditions during the studied period have been previously described in detail (Chubarova et al., 2021; Vlasov et al., 2023a). In summary, the air temperature in April and May was lower compared to the 1954–2013 period by 1.4 °C and 1.7 °C, respectively, due to the prevailing air advection from northern regions (Chubarova et al., 2021), while in June it was higher by 1.5 °C (Chubarova et al., 2014).

The year 2020 was unique in terms of precipitation patterns. In April, the precipitation amount was 2.4 times lower than the annual average (17 mm compared to 41 mm). However, unprecedented precipitation (168 mm and 193 mm) in May and June was almost three times higher than a long-term monthly mean (55 mm and 76 mm for May and June, respectively). In July, there was 113 mm of precipitation, exceeding the average of 81 mm. As a result, the significant amount of precipitation during late

spring and early summer contributed to the purification of the atmosphere from pollutants (Vlasov et al., 2023a). The amount of daily precipitation is shown in Fig. S2. For rainfall lasting more than a day, the amount of water was measured at the end of the last day. For such cases, the volume of daily precipitation was calculated as half (if the rain lasted two days) or one-third (if the rain lasted three days) of the total amount of water over the entire period. Such situations occurred on May 3–4, 5–6, 12–14 and 24–25, June 25–26, and July 3–4.

Chemical analyses and data processing

Concentrations of Al, As, B, Ba, Bi, Ca, Cd, Co, Cr, Cs, Cu, Fe, K, Li, Mg, Mn, Mo, Na, Ni, P, Pb, Rb, S, Sb, Sn, Sr, Th, Ti, U, V, W, Zn, and Zr were determined by mass spectrometry and atomic emission spectrometry with inductively coupled plasma, using the “X-7c” mass spectrometer (Thermo Elemental, USA) and “iCAP-6500” atomic emission spectrometer (Thermo Scientific, USA), respectively, at the Analytical Certification Testing Center of the Institute of microelectronics technology and high purity materials of the Russian Academy of Sciences. Reference materials “GSO 3784-86”, “GSO 8670-2005”, and “GSO 8671-2005” (Vinogradov Institute of Geochemistry SB RAS, Russian Federation) as well as “AGV-2” and “BHVO-2” (U.S. Geological Survey, USA) were used. A detailed description of the sample preparation procedure, a list of reagents used, and instrument settings are given in (Fedotov et al., 2014). The detection limits are shown in Table 1. Uncertainties are in the range of 10–30% depending on the element concentration.

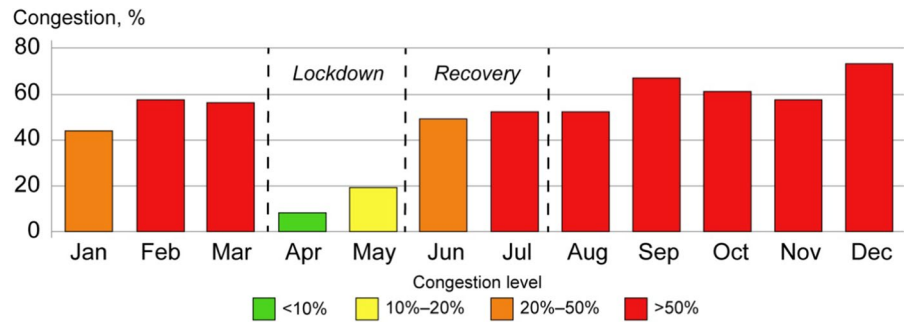
Changes in PTEs concentrations (δ_m , %) during the studied periods relative to each other were calculated as follows:

$$\delta_m = 100\% \times (C_m - C_{m-1}) / C_{m-1}, \quad (1)$$

where C_m and C_{m-1} are the median PTE concentrations during the m th period and the previous one, respectively. Median values were used for the study instead of averages due to the high variability of PTE concentrations.

PTE sources in PM₁₀ were assessed using an enrichment factor (E_{Fi}):

Fig. 2 Average monthly congestion level in Moscow in 2020 (TomTom Traffic Index, 2020)



$$EF_i = (C_i/C_{Al})/(K_i/K_{Al}), \quad (2)$$

where C_i and C_{Al} are the concentrations of the i th and reference (Al) elements in the PM_{10} sample, respectively, and K_i and K_{Al} are the abundances of the i th and reference (Al) elements in the upper continental crust, respectively (Rudnick & Gao, 2014). The reference element should not originate from anthropogenic sources, and Al is the most often used. $EF < 10$ indicates a natural origin of elements, EF values from 10 to 100 indicate mixed natural and anthropogenic sources, and $EF \geq 100$ is inherent for elements of entirely anthropogenic origin (Chon et al., 2015). Total enrichment factor TEF was calculated for an integral assessment of the degree of PTEs accumulation (Vlasov et al., 2021b):

$$TEF = \sum_{i=1}^n EF_i - (n - 1), \quad (3)$$

where n is the number of summable individual elements with $EF > 1$.

Health risks associated with PM_{10} -bound PTEs were estimated using U.S. EPA standards (U.S. EPA, 2011, 2013, 2014). For particle-bound chemical compounds, inhalation is a primary and the most significant exposure route (Fang et al., 2021), so in our study, we considered the health risks associated with the inhalation of selected PTEs. Children and adults were studied separately because of their different sensitivities to toxicity. Twenty-one elements (Al, As, B, Ba, Cd, Co, Cr, Cu, Fe, Mg, Mn, Mo, Ni, Pb, Sb, Sn, Ti, U, V, W, and Zn) were considered as toxic substances, and six elements (As, Cd, Co, Cr, Ni, and Pb) were ranked as carcinogens or possible carcinogens in terms of U.S. EPA (2022) and the Ministry of Health of the Russian Federation

(Rakhmanin et al., 2004). Due to the difference in toxicity between ions with different valencies, the concentration of Cr^{6+} was calculated as one-seventh of the total chromium concentration (Wang et al., 2021d).

The non-carcinogenic risk was defined as:

$$HQ_j = (C_j \times InhR \times EFR \times ED) / (BW \times AT \times RfD_j \times 10^6), \quad (4)$$

$$HI = \sum HQ_j, \quad (5)$$

where HQ_j is the hazard quotient of the j th element (unitless); C_j represents the concentration of the j th toxic element in PM_{10} (ng/m^3); $InhR$ is the inhalation rate (m^3/day) and is used separately for children up to 6 years old ($InhRc$) and adults from 21 to 71 years old ($InhRa$); EFR represents the exposure frequency ($day/year$); ED is the exposure duration (year) which is determined separately for children (EDc) and adults (EDa); BW is body weight (kg) of a child (BWc) or adult (BWa); AT is the average time (day); RfD_j is the reference dose of the j th element ($mg/kg/day$); 10^6 is conversion factor (ng/mg); HI is the hazard index (unitless). $InhR$, EF , ED , BW , and AT values are shown in Table S1 (Supplementary materials).

The carcinogenic risk was calculated as follows:

$$CR_j = (C_j \times EFR \times SF_j / (AT \times 10^6)) \times (InhRc \times EDc / BWc + InhRa \times EDa / BWa), \quad (6)$$

$$TCR = \sum CR_j, \quad (7)$$

where CR_j refers to the carcinogenic risk of the j th element (unitless); SF_j represents the slope factor of the j th element ($kg \times day/mg$); TCR is the total carcinogenic risk (unitless). The values of RfD_j and SF_j

Table 1 Descriptive statistics of PM₁₀-bound PTEs during lockdown (L) and recovery (R) periods in April–July 2020

PTE	Detection limit, ng/filter	Lockdown period L (Apr 24–May 31), <i>n</i> =29			Recovery period R (Jun 01–Jul 30), <i>n</i> =40		
		Mean ± s.d., ng/m ³	Min–Max, ng/m ³	<i>Cv</i> , % (NDL, %)	Mean ± s.d., ng/m ³	Min–Max, ng/m ³	<i>Cv</i> , % (NDL, %)
Li	0.35	0.18 ± 0.088	0.07–0.40	48	0.22 ± 0.10	0.067–0.51	48
B	3.4	0.62 ± 0.35	0.12–1.4	56 (7)	1.2 ± 0.73	0.12–2.7	62 (2)
Na	190	62 ± 36	11–140	58	66 ± 29	21–168	44
Mg	23	54 ± 26	16–116	48	66 ± 44	17–268	67
Al	97	158 ± 70	53–299	44	162 ± 92	29–410	57
P	150	12 ± 5.9	5.0–29	47 (31)	19 ± 6.7	5.1–32	36
S	270	294 ± 146	62–658	50	373 ± 261	77–1405	70
K	63	72 ± 33	22–136	45	98 ± 44	35–190	45
Ca	540	464 ± 197	151–957	42	554 ± 274	162–1138	50
Ti	19	9.8 ± 8.8	1.5–32	90	12 ± 7.1	0.75–34	59
V	5.1	0.72 ± 0.49	0.17–2.2	68 (17)	0.85 ± 0.695	0.17–2.9	82 (20)
Cr	5.3	3.4 ± 1.1	1.4–6.1	32	5.1 ± 1.6	2.9–9.9	30
Mn	3.9	5.8 ± 2.3	2.4–11	40	8.6 ± 3.9	2.9–20	46
Fe	140	291 ± 122	123–690	42	425 ± 210	113–1111	49
Co	0.7	0.10 ± 0.053	0.024–0.26	52 (14)	0.12 ± 0.063	0.025–0.33	53
Ni	3.8	0.68 ± 0.59	0.15–2.7	86	0.56 ± 0.30	0.16–1.4	54
Cu	5.8	5.3 ± 2.7	1.9–14	50	11 ± 9.3	2.7–49	87
Zn	7.4	14 ± 10	4.1–61	77	16 ± 8.0	5.5–46	50
As	0.55	0.053 ± 0.098	0.018–0.49	184 (83)	0.096 ± 0.12	0.010–0.46	124 (60)
Rb	0.48	0.35 ± 0.18	0.10–0.84	52	0.43 ± 0.24	0.12–0.97	55
Sr	0.69	1.4 ± 0.71	0.54–3.1	49	1.8 ± 0.93	0.53–4.1	51
Zr	0.48	0.4 ± 0.18	0.19–0.83	44	0.71 ± 0.49	0.19–2.2	70
Mo	0.45	0.20 ± 0.21	0.054–1.1	107	0.37 ± 0.24	0.12–1.3	65
Cd	0.26	0.13 ± 0.11	0.009–0.42	78 (3)	0.16 ± 0.26	0.009–1.7	162 (5)
Sn	1.1	1.1 ± 1.1	0.30–5.9	99	2.8 ± 2.6	0.49–12	94
Sb	0.3	0.93 ± 0.79	0.19–3.9	85	1.5 ± 1.8	0.28–10	117
Cs	0.064	0.024 ± 0.022	0.002–0.11	95 (3)	0.031 ± 0.03	0.002–0.12	95 (7)
Ba	0.24	5.4 ± 2.3	2.3–13	42	11 ± 5.5	2.5–28	51
W	0.2	0.15 ± 0.11	0.029–0.48	72	0.096 ± 0.051	0.035–0.24	54
Pb	0.35	4.7 ± 4.3	0.55–17	91	6.6 ± 6.2	0.96–28	94
Bi	0.097	0.065 ± 0.067	0.028–0.39	102	0.13 ± 0.087	0.022–0.41	67
Th	0.05	0.022 ± 0.013	0.005–0.054	58	0.027 ± 0.016	0.005–0.07	62
U	0.014	0.01 ± 0.005	0.003–0.02	48	0.012 ± 0.006	0.003–0.024	52

n is the number of samples. NDL is the percentage of samples with a concentration below the detection limit of the total number of samples for the period; NDLs of 0% are not shown. *Cv* is the coefficient of variation, and *Cv* > 70% are given in bold

are based on the data of the U.S. EPA, Cal EPA, and the Ministry of Health of the Russian Federation (Cal EPA, 2022; Rakhmanin et al., 2004; U.S. EPA, 2022) and are listed in Table S2 (Supplementary materials).

For non-carcinogenic risk *HQ* and *HI* are classified as: no hazard (<0.1), low hazard (0.1–1),

moderate hazard (1–10), and high hazard (>10) (Lemly, 1996). For carcinogenic risk, *CR* and *TCR* values are classified into four grades: very low (≤10⁻⁶), low (10⁻⁶–10⁻⁴), medium (10⁻⁴–10⁻³), high (≥10⁻³) risk (Rakhmanin et al., 2004).

Identification of main PTEs sources was based on the absolute principal component analysis with multiple linear regression (APCA-MLR) in Statistica 8 (TIBCO Software Inc., USA) and R programming environment. The contribution of sources to the PTE concentrations was determined using the PCA with the calculation of Absolute Principal Component Scores (APCS). The detail process of APCA-MLR modeling was described in Thurston and Spengler (1985). The main steps of the approach are summarized below. Prior to the analysis, Z-normalization was applied:

$$Z_{ik} = (C_{ik} - \bar{C}_i) / \sigma_i, \quad (8)$$

where C_{ik} is the concentration of the i th chemical element in the sample k , \bar{C}_i is the average concentration of the i th element, and σ_i is the standard deviation of the i th element.

The Varimax rotation method for PCA was used. Kaiser–Meyer–Olkin (KMO) and Bartlett's sphericity tests were performed to examine the suitability of the data for PCA (Varol, 2011). Only the principal components with eigenvalues > 1 (Kaiser's criteria) were used as factors. As the factor scores obtained from PCA are normalized, with mean zero and standard deviation equal to unity, the true zero for each factor score was calculated by introducing an artificial sample with zero concentrations of all variables. For this additional sample, normalized values for PTE concentrations will be as follows:

$$(Z_0)_i = (0 - \bar{C}_i) / \sigma_i = -\bar{C}_i / \sigma_i. \quad (9)$$

The APCS for each component are then estimated by subtracting the factor scores for this artificial sample from the factor scores of each one of the true samples.

Regressing the PTE concentration data on APCS gives estimates of the coefficients, which convert the APCS into pollutant source mass contributions of each source for each sample. The source contributions to C_i can be calculated as follows:

$$C_i = \xi_{0i} + \sum (APCS_p \times \xi_{pi}), p = 1, 2, \dots, n, \quad (10)$$

where ξ_{0i} is the intercept of multiple regression for the i th element, ξ_{pi} is the coefficient of multiple regression of the source p for pollutant i , and $APCS_p$ is the scaled value of the rotated factor p for the considered

sample. $APCS_p \times \xi_{pi}$ represents the contribution of source p to C_i . The mean of the product $APCS_p \times \xi_{pi}$ for all samples represents the average contribution of the sources (Ma et al., 2021).

APCA-MLR uncertainty (UNC, %) is calculated as:

$$UNC = (C_{meas} - C_{model}) / C_{meas} \times 100\%, \quad (11)$$

where C_{meas} is the measured concentration of PTE, and C_{model} is the predicted concentration of PTE based on APCA-MLR (Song et al., 2006).

Results and discussion

PTE concentrations during the lockdown and recovery periods

Descriptive statistics for concentrations of PM₁₀-bound PTEs in Moscow during the lockdown (L) and recovery (R) periods in April–July 2020 are shown in Table 1. During the L period, the statistical analysis revealed a high coefficient of variation (C_v) for As, Mo, Bi (102–184%), and for Sn, Cs, Pb, Ti, Sb, Ni, Cd, Zn, W (72–99%). For other elements, the C_v ranged from 32 to 68%. The resumption of anthropogenic impact after the lifting of restrictions resulted in increased C_v for Cd, Cu, Sb, S, V, Zr, Al, and Mg concentrations by 12%–83%.

The time series (Fig. S3, Supplementary materials) depict peaks in PTE concentrations during the L1 period, which were observed on April 26 and likely associated with the advection of polluted air. Additional peaks were noted at the beginning and the end of the first decade of May, coinciding with the traditional burning of large amounts of garbage and fuel in suburban areas during the May holidays, as well as a large number of barbecues held in city parks. Following the end of the heating season, peaks of PTE concentrations in the L2 period were recorded on May 15–16 and May 28. After the beginning of restrictions removal (L2), the concentrations of most PTEs began to increase rapidly, reaching maxima on June 8–10 and June 16–18. This may be attributed to the smoke transfer from the suburbs, as earlier an advection of a smoke cloud from agricultural fires was confirmed for June 18 (Chubarova et al., 2021). During these advection events, industrial enterprises that continued

to operate in cities near Moscow could exert an additional impact (Vergel et al., 2022). Notable increases in PTEs concentrations were observed on June 22–24 and July 26–27, with specific days (July 4, 6, 10, 12, and 19) showing elevated levels of Sb, Sn, As, Cu, B, Cs, Pb, Mo, Bi, and Zr.

In the recovery period R, the values of C_v decreased for As, Mo, Bi, Ni, Ti by 31–61%, and for W, Zn, Na, P by 12%–27% because of either the growth of average concentrations in period L or a reduced range between maximum and minimum concentrations due to a rapid increase in minimum concentrations compared to maximum ones. PTEs originating from crustal sources, i.e., B, Ba, Ca, Co, Cr, Fe, K, Li, Mn, Rb, Sr, Th, and U, showed 10% and lower differences in C_v between L and R periods. In general, after the removal of restrictions, higher C_v were observed for Cd, As, and Sb (117–162%) and Cs, Pb, Sn, Cu, Mo, V, S, and Zr (70–95%). C_v for other elements varies from 30 to 67%, indicating that they come from mixed sources.

The δ_m coefficient shows a significant increase in the concentrations of nearly all PTEs in the R period compared to the L period (Fig. 3). The most significant growth ($\delta_1 > 100\%$) is typical for Bi, Mo, and Sn, and less pronounced (δ_1 from 40 to 100%) for Ba, B, Ti, Cu, Sb, Zr, and Cr, which indicates the supply of all above-listed PTEs predominantly from anthropogenic sources. The increase in anthropogenic activities during the R period is supported by data on rising combustion of fossil fuels in Moscow, accompanied by the recovery of traffic intensity and revival of the energy and industrial sectors almost immediately after the start of restrictions removal (Popovicheva et al., 2022). Relatively modest increases in δ_1 , ranging from 10 to 40%, were recorded for Fe, Zn, P, Mn, K, Pb, Sr, Cs, and Na. Only W exhibited a clear decrease in concentrations after the removal of restrictions ($\delta_1 = -36\%$), which can be attributed to the typically high W levels for Moscow in atmospheric aerosols in spring and its minimal occurrence during the summer compared

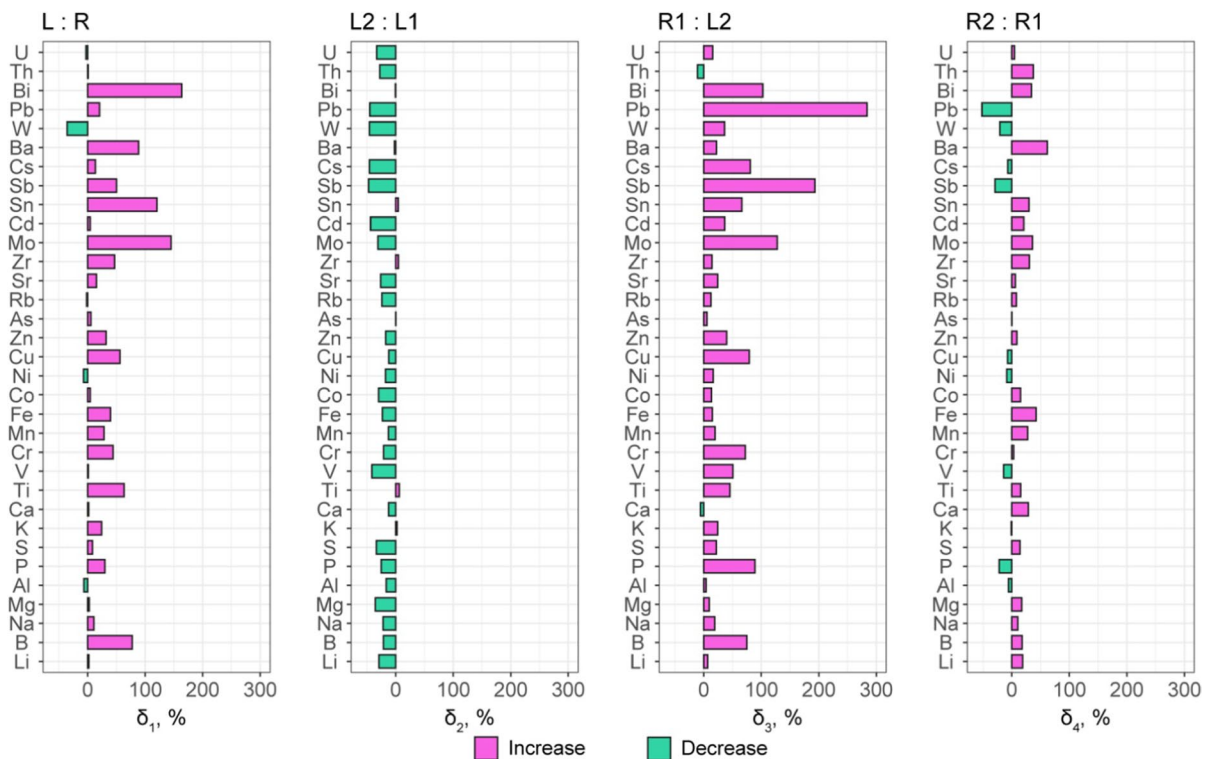


Fig. 3 Changes in median concentrations ratio (δ_m , %) of PM_{10} -bound PTEs in Moscow during the periods L, R, L1, L2, R1, and R2. Coefficients $\delta_m = 100\% \times (C_m - C_{m-1})/C_{m-1}$ show

changes in PTE concentrations C_m and C_{m-1} during the m th period as compared to the previous one

to other seasons, as previously observed in the city center (Gubanova et al., 2021a). As for the content of PM₁₀-bound Al, As, Ca, Cd, Co, Li, Mg, Ni, Rb, S, Th, U, and V, the differences between R and L did not exceed $\pm 10\%$.

Comparison of the periods L2 (lockdown period after the end of the heating season) and L1 (lockdown period during the heating season) allowed assessing the atmosphere state under minimal anthropogenic impact. During L2, there was a rapid decrease in the concentrations of most PTEs due to the end of the heating season and high precipitation in May, reaching up to 20 mm per day (Fig. S2, Supplementary materials). The decrease ranged from 30 to 50% for Pb, W, Sb, Cd, S, V, Cs, Co, Li, U, and Cr and from 10 to 30% for other elements, except K, Ba, As, Ti, Ca, P, and Mn. The latter changed their concentrations by no more than 10%. The concentration of Bi increased by 18% (Fig. 3). The increased atmospheric oxidizing capacity during the lockdown promoted the formation of more acidic species and further enhanced the dissolution of aerosol PTEs (Liu et al., 2021), which, along with heavy rains, may be a reason for the decrease of PTE concentrations in the air during the lockdown.

The comparison of R1 and L2 periods shows a rapid increase in the concentrations of nearly all PM₁₀-bound PTEs during R1 after the beginning of the removal of restrictions, especially for Pb, Sb, Mo (by 122–244%), Cu, Bi, Sn, Cr, B, P, Cs, Ti, and V (by 43–84%), Zn, Cd, Zr, W, K, Sr (by 20–31%), indicating a crucial role of anthropogenic sources in PTE air pollution in Moscow and a significant impact of restrictive measures on the abatement of the overall atmospheric pollution with PTEs. The increase in concentrations of other pollutants was 10–20% and did not exceed 10% for As, Al, Mg, and Li; concentrations of Ca and Th decreased by 12–17% after the removal of restrictions.

Comparison of periods R2 and R1 makes it possible to estimate the duration of PTE air pollution recovery. During R2, the concentrations of most PTEs such as Ba, Fe, Th, Mo, Bi, Zr, Sn, Ca, and Mn ($\delta_4=27\text{--}63\%$), as well as Cd, Li, B, Mg, Ti, Co, S, and Na ($\delta_4=10\text{--}21\%$) continue to increase, that is, the time lag between the lifting of restrictions and the restoration of the level of PM₁₀-bound PTEs exceeds two weeks (the duration of the R1 period). The prolonged lag, as well as the decrease in the concentrations of

V, W, P, Sb, and Pb by 14–52% during R2 relative to R1, is probably associated with (1) the beginning of the vacation season and the significant departure of a large number of residents outside the city and suburbs to other regions, and (2) frequent and heavy rains in R1, the first weeks of R2 and occasionally in July, which hindered the full recovery of pollutant levels in the air. The values of δ_4 do not exceed $\pm 10\%$ for Al, As, Cr, Cs, Cu, K, Ni, Rb, Sr, U, and Zn, indicating the stabilization of the levels of these PTEs after the complete cancellation of restrictive measures.

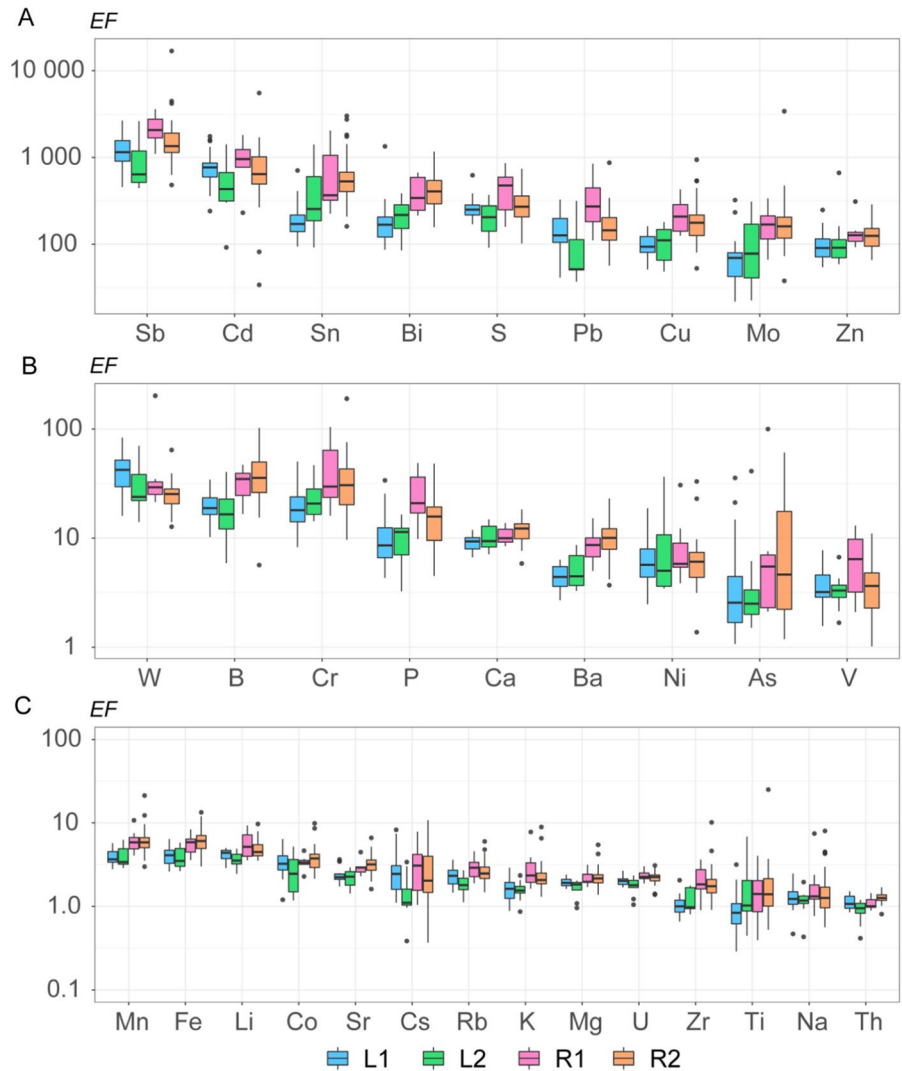
The decreasing trends of PM₁₀-bound PTE concentrations obtained for Moscow are close to the results obtained for PM_{2.5} in Tangshan, China, where during the lockdown, concentrations of Zn, Pb, and Cr decreased by 39%–48%, Fe by 25%, and Cu by 7% (Li et al., 2021). Concentrations of Cr, Pb, Mn, Fe, Zn, As, and Ni in PM_{2.5} in Taiyuan, China, decreased by 39–51% (Wang et al., 2021c), which is slightly below the estimates for PM₁₀ in Elche, Spain, for K, Ca, Ti, Mn, Fe, Ni, Cu, and Zn (40–80%) coming from road dust and worn out brake particles (Clemente et al., 2022).

Enrichment factors

EF determines the levels of enrichment of atmospheric aerosols with PTEs in different periods and the probable origin of the elements (Fig. 4). A high median level of $EF \geq 100$ for Sb, Cd, Sn, Bi, S, Cu, and Zn during the all four studied periods indicates the dominant influence of anthropogenic sources. The *EF* values for these PTEs increased after the restrictions were removed, especially for Sb, Cd, S, Pb, Cu, Mo, and Zn during R1, and for Sn and Bi during R2 (Fig. 4A), which suggests that various sources resumed their activities at different rates following the lockdown.

During all periods, *EFs* are 10–100 for W, B, Cr, and Ca (Fig. 4B). During the recovery periods R1 and R2, $EFs > 10$ were also observed for P and Ba. Almost all PTEs exhibited an increase in *EFs* after the removal of restrictive measures, indicating a mixed origin from both natural and anthropogenic sources. A decrease in *EFs* was noted for W from the start of restrictions to the recovery period, which aligns with the previously identified similar trend in the *EFs* of this metal in Moscow aerosols from spring to summer (Gubanova et al., 2021a).

Fig. 4 Enrichment factors for PM₁₀-bound PTEs from **A** anthropogenic sources with *EF* > 100, **B** mixed natural and anthropogenic sources with *EF* from 10 to 100, and **C** natural sources with *EF* < 10 during April–July 2020. The boxes show the 25% and 75% quartiles, and the whiskers show the minimum and maximum values



*EF*s < 10 for Ni, As, V, Mn, Fe, Li, Co, Sr, Cs, Rb, K, Mg, U, Zr, Ti, Na, and Th indicates the dominance of natural (terrigenous) sources during all periods (Figs. 4B, 4C). After the removal of restrictions, *EF*s of these elements increased, similar to the anthropogenic PTEs, possibly due to meteorological conditions. In the summer months, especially during R2, the blowing of soil particles and road dust became more intense as compared to spring due to higher air temperatures and prolonged dry periods between sporadic rains in July (Gubanova et al., 2022). The enrichment of PM₁₀ particles with elements of terrigenous origin can also be amplified due to the growth of the number of cars on the roads, which contribute to the accelerated formation

of road dust particles and their active blowing in Moscow (Ivaneev et al., 2023).

Throughout all periods, the association of PTEs with the highest *EF*s was stable, and it included Sb, Cd, Sn, Bi, S, Pb, Cu, Mo, and Zn. This set closely aligns with the list of PTEs that accumulate in aerosols in different seasons (Gubanova et al., 2021a), in soils (Kosheleva et al., 2018; Romzaykina et al., 2021; Vlasov et al., 2022), road dust and its PM₁₀ fraction (Ermolin et al., 2018; Ivaneev et al., 2023; Kasimov et al., 2020; Ladonin & Mikhaylova, 2020; Vlasov et al., 2023b), dissolved and suspended phases of snow cover (Vinokurov et al., 2017; Vlasov et al., 2020) and atmospheric precipitation (Vlasov et al., 2021a, 2023a), river suspension, water, and bottom

sediments (Erina et al., 2021; Shinkareva et al., 2022; Vlasov et al., 2019). This testifies to forming a cohesive geochemical profile of anthropogenic impact in almost all components of the urban environment in Moscow.

The total enrichment factor (*TEF*) provides a comprehensive assessment of aerosol enrichment with PTEs (Fig. 5A, B) and their contribution to PM_{10} pollution (Fig. 5C, D). During the lockdown period L1, the *TEF* values varied from 1549 to 4820. During L2, after the end of the heating season until the last week of May, *TEF* did not exceed 2700, then it increased immediately after the start of restrictions removal, and it amounted to 9239 on June 3. The growth of *TEFs* during the last week of May could be a result of the anomalous precipitation that contributed to the removal of large particles from the atmosphere (Vlasov et al., 2023a). A total of 121 mm of precipitation fell out from May 28 to June 2 (Fig. S2, Supplementary materials), which is double the monthly norm for May (Chubarova et al., 2014). Moreover, aluminum, used as a normalizing element in calculating *EFs*, is usually associated with large particles

(Guo et al., 2015). Thus, June 3 marked the minimum concentration of Al (40 ng/m^3) and the maximum *TEF* in April–June. The essential role of precipitation in cleaning the air was also noted in the State of São Paulo, Brazil, where heavy rains prior to the introduction of restrictive measures led to only a slight reduction in air pollution with gases, PM_{10} and $PM_{2.5}$ particles during the lockdown itself (Rudke et al., 2021).

During the first weeks of the recovery period R1, the *TEF* gradually decreased to 5536. Throughout R2, the *TEF* varied from 2518 to 5308 until July (Fig. 5A). In July, the pattern of *TEF* change is similar to a “heart rate”-shaped one with alternating peak and low values. Such variability in *TEF* is typical only for the period after the removal of restrictive measures. Local *TEF* peaks were observed on July 6 ($TEF=22,784$), July 15 (14,108), July 17 (8102), and July 27 (12,058). The peaks of July 15 and July 17 coincided with a period of heavy rains on July 14–17, when 44 mm of precipitation fell out (almost half of the monthly norm for July), and it was on July 15 that the minimum Al concentration (28 ng/m^3) for the entire study period in April–July was recorded (28

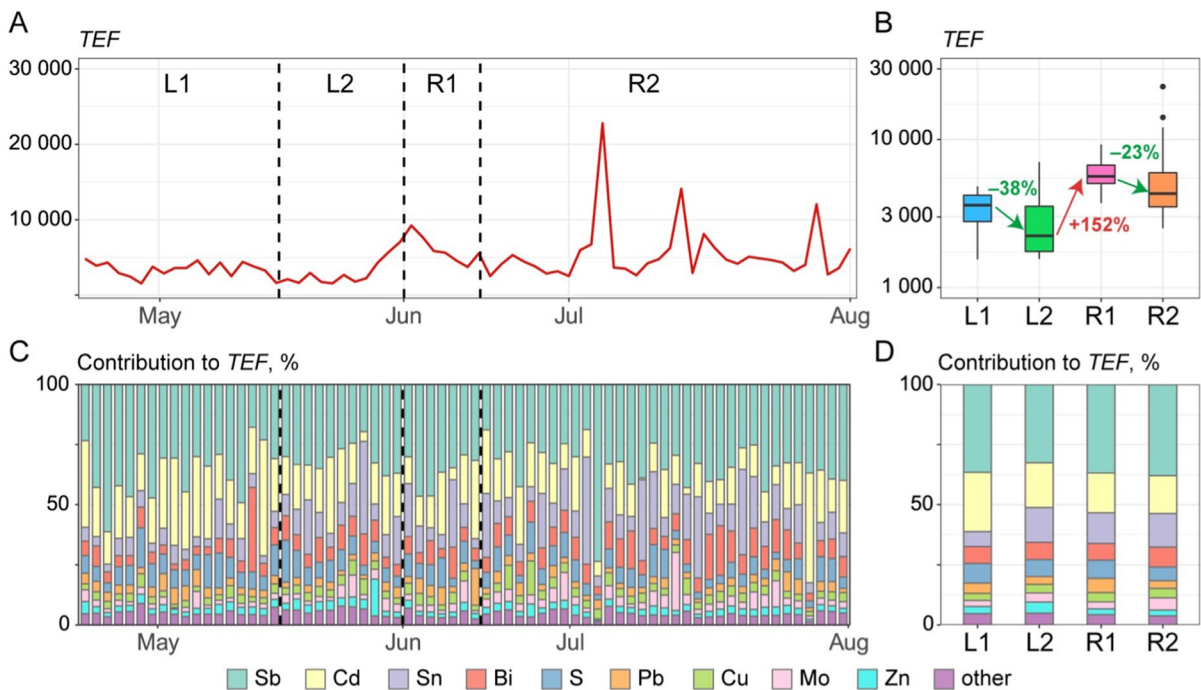


Fig. 5 Total enrichment factor: **A** daily variations of *TEF* during April–July 2020, **B** mean, 25% and 75% quartiles, and the minimum and maximum values of *TEF* for the studied periods,

C contributions of selected elements to *TEF* during April–July 2020, and **D** mean contributions of selected elements to *TEF* for the studied periods

ng/m³). The peak of July 27 corresponds to a relatively heavy rain of 8.5 mm. In other episodes, significant changes in *TEF* during precipitation were not recorded.

Comparison of median *TEF* values in the four studied periods revealed a change in the total aerosol enrichment with PTEs during and after the removal of restrictions (Fig. 5B). In the second period of restrictions L2, *TEF* decreased by 38% compared to L1. The removal of restrictions had a rather strong impact on the overall level of PTEs in aerosol: in the period R1, *TEF* increased by 152% compared to L2, and after the complete removal of restrictions in R2, there was a decrease of 23%. Wherein more than 1/3 of the *TEF* value during April–July was accounted for by Sb (Fig. 5C), and together with Cd, these two elements determined more than half of the *TEF* value. Among other elements, Sn, Bi, S, Pb, Mo, and Zn contributed most ($\geq 5\%$) to the *TEF* in certain periods studied. During L2 after the end of the heating season, the contribution of Sb and Cd (Fig. 5D) to *TEF* decreased mainly due to a significant increase in the share of Sn (from 6 to 14%). In the period R1, the input of Sb, S, and Pb to *TEF* began to grow, while the proportion of Cd, Sn, Mo, and Zn became lower. After the complete removal of restrictions in R2, the contribution of Sb, Bi, Mo, and Sn slightly increased, and that of Cd, S, and Pb decreased. This indicates a change in the sources of PTEs and their role in the overall pollution of aerosols.

Source identification with APCA-MLR

To identify possible sources and apportion the PM₁₀-bound PTEs during the lockdown in Moscow, the APCA-MLR method was used. PTEs with strong ($r > 0.9$) correlations (Fig. S4, Text S1, Supplementary materials) were excluded from the analysis to prevent confounded effects as suggested earlier (Ashton & Macintosh, 2002; Pinto & Maheshwari, 2011): Li, Th, U (high r with Al), Mg and Sr (Ca), Mn and Ba (Fe), Rb (K, Cs), Al (Ca), as well as As and P as having more than 80% and 30% of samples with concentrations below the DL during the lockdown period, respectively (Table 1). APCA-MLR analysis was applied to a single dataset that included the results of sixty-nine PM₁₀ samples testing for the content of twenty-two PTEs. Kaiser–Meyer–Olkin test (0.80, meritorious level) and Bartlett’s sphericity

test ($p < 0.001$) showed the suitability of the dataset for PCA (Varol, 2011).

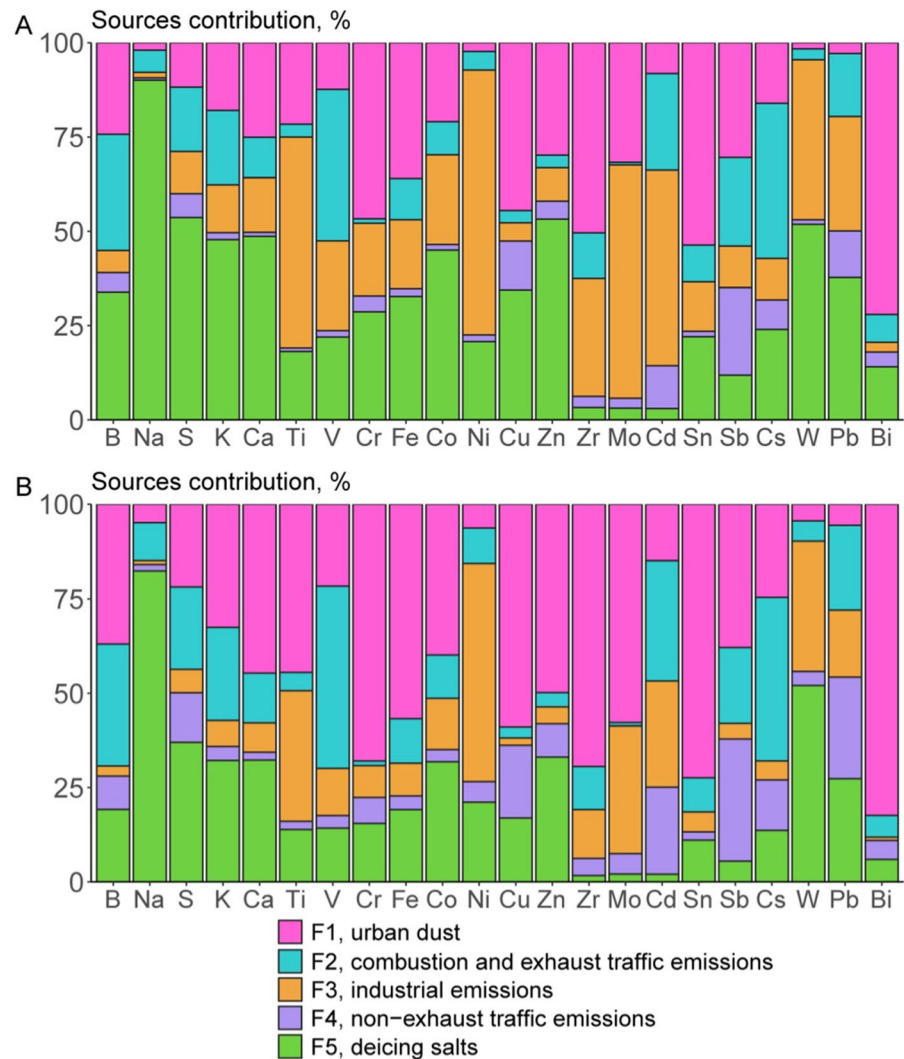
PCA with Varimax rotation revealed five principal components (Table S3, Supplementary materials) that explained 70.5% of the total PTEs variance: PC1 (19.3% of total variance) is associated mainly with the accumulation of Bi–Fe–Sn–Zr–Cr–Ca–Cu; PC2 (18.3% of total variance) explains the accumulation of V–Cs–K–B–S; PC3 (11.5% of total variance) relates predominantly to Ni–W–Ti–Mo; PC4 (12.2% of total variance) is associated with Sb–Cu–Pb; PC5 (9.2% of total variance) connected predominantly with Na.

The specific contribution rates of different sources to PTEs concentrations, obtained through APCA-MLR analysis and averaged for the entire study period, are presented in Table S4 (Supplementary materials). The values of the coefficient of determination R^2 between the initial concentrations of PM₁₀-bound PTEs and the estimated concentrations were > 0.5 for all elements (> 0.6 in most cases). The uncertainty in the estimates did not exceed $\pm 25\%$ for all elements except Ti and Cr (31% and 40%, respectively). These results indicate a good agreement between the modeled and observed values and demonstrate the reliability of the source contribution estimates (Haji Gholizadeh et al., 2016). During the APCA-MLR, we assumed that each factor associated with the influence of the PTEs source corresponds to the identified principal component (for instance, F1 corresponds to PC1, F2 corresponds to PC2, etc.).

To assess changes in the contributions of possible sources after the removal of restrictions, the average contributions of PTEs to PM₁₀ composition were calculated for the lockdown L and recovery R periods (Fig. 6).

For the lockdown period L, the *first factor*, i.e., *urban dust*, has component loadings > 0.5 with Bi, Fe, Sn, Zr, Cr, Ca, and Cu and is responsible for high concentrations of PM₁₀-bound K, B, Ti, Co, Zn, Mo, Sn, and Sb (Table S4) with component loadings < 0.5 . The factor is probably associated with the transport of urban dust, including particles of polluted soils, construction dust, mineral particles, fine fractions of road dust, etc. (Fig. 6). Calcium is an indicator of carbonate dust, often emitted in cities during construction and demolition processes (Ramírez et al., 2019). The association connected with the first factor shows a similar composition to Moscow road dust and its

Fig. 6 Source contribution to PM₁₀-bound PTEs in April–July 2020: **A** during the lockdown, **B** after the lockdown



PM₁₀ fraction, which are highly enriched with Bi, Cu, Sn, Sb, Mo, and Zn (Vlasov et al., 2021b). High concentrations of K, Ti, Fe, Zr, and Co are characteristic of the composition of secondary soil minerals (Kabata-Pendias, 2011), while Zr, Ca, Cr, Fe, Sb, Ti, and Co are released when the road surface and car parts are worn out by transport (Pant & Harrison, 2013).

The *second factor* is related to the *combustion and exhaust traffic emissions*. It is associated with V, Cs, K, B, and S. The input of K, Cs, and S may be due to the combustion of biomass, garbage, and fossil fuels (Christian et al., 2010; Landing et al., 2010; Massimi et al., 2020). Vanadium is a component of lubricating oils and can be found in diesel emissions

(Shafer et al., 2012), borates are widely used to produce automotive fluids (U.S. Borax, 2023). Factor 2 is not associated with the supply of soil particles and crustal materials, as the K/Cs ratio in the factor 2 profile is 1481 (Table S4), which is 3.2 times lower than that in the Earth's crust (Rudnick & Gao, 2014), and 2.3 times lower than in the profile of the first factor. This prevents identification of the second factor as a supply of soil particles and crustal materials, despite the relatively high concentrations of K and Na in the factor 2 profile compared to the other factors. However, relatively high Na emission factors are typical for passenger cars, even of the Euro-4 class (Alves et al., 2015).

The *third factor* indicates *industrial emissions*; it has high component loadings for Ni, W, Ti, and Mo, as well as high concentrations of Cd and Pb in the profile of this factor relative to other factors. Factor 3 characterizes the impact of industrial facilities, especially metalworking enterprises and repair shops, and is associated with the abrasion of steel products (Bencharif-Madani et al., 2019; Bozkurt et al., 2018). Their influence is confirmed by the Mo/Sb ratio of 1.8 for factor 3 and 0.01–0.34 for other factors (Table S4). We have previously proved that industrial pollution of dust in Moscow is clearly traced by Mo/Sb > 1 (Vlasov et al., 2021b).

The *fourth factor* is related to *non-exhaust traffic emissions* associated with the contribution of Sb, Cu, and Pb. These elements are released into the atmosphere when the brake mechanisms of cars are abraded (Ozaki et al., 2021; Ramírez et al., 2019); they show high concentrations in PM₁₀ fraction of road dust in Moscow (Vlasov et al., 2021a) and urban soils (Kosheleva et al., 2018; Vlasov et al., 2022). The Cu/Sb ratio for F4 is 4.9, which falls within the range of 2.2–18.9 observed in atmospheric particles in tunnels and road dust in various cities (Alves et al., 2018). The Zn/Cu ratio (0.6) is minimal for F4; for other factors, it is 1.5–6 times higher, which proves the transport source of Cu (Hwang et al., 2016). Brake pad abrasion produces particles with the Fe/Cu ratio between several unities and 40 (Alves et al., 2018). In our study, the Fe/Cu ratio for F4 is minimal (7) compared to other factors (35–162), which also supports the identification of F4 as non-exhaust traffic emissions.

The *fifth factor* indicates *deicing salts*; it has high component loading for Na. High S, K, Ca, Co, W, and Pb concentrations also characterize its profile. Blowing out of particles of deicing mixtures (NaCl, CaCl₂, or marble chips) used for roadway treatment in the cold period in Moscow (Voronov et al., 2019) impacts the ion composition of aerosols as well (Zappi et al., 2023). Salt remains on the road surface even after heavy rains in summer, causing an increased electrical conductivity of road dust (Kasimov et al., 2019) and salinity of the surface horizon of urban soils (Nikiforova et al., 2014). Additionally, factor 5 may be associated with the formation and transport of a secondary inorganic aerosol due to the lowest S/Na ratio (3) compared to other factors (15–51) and high concentrations of S in the F5 profile that may indicate

sulfate-rich aerosols (Grivas et al., 2018). Factor 5 is also characterized by increased concentrations of Zn, Co, and Fe (Table S4), the accumulation of which can be contributed by secondary aerosols (Wang et al., 2021a).

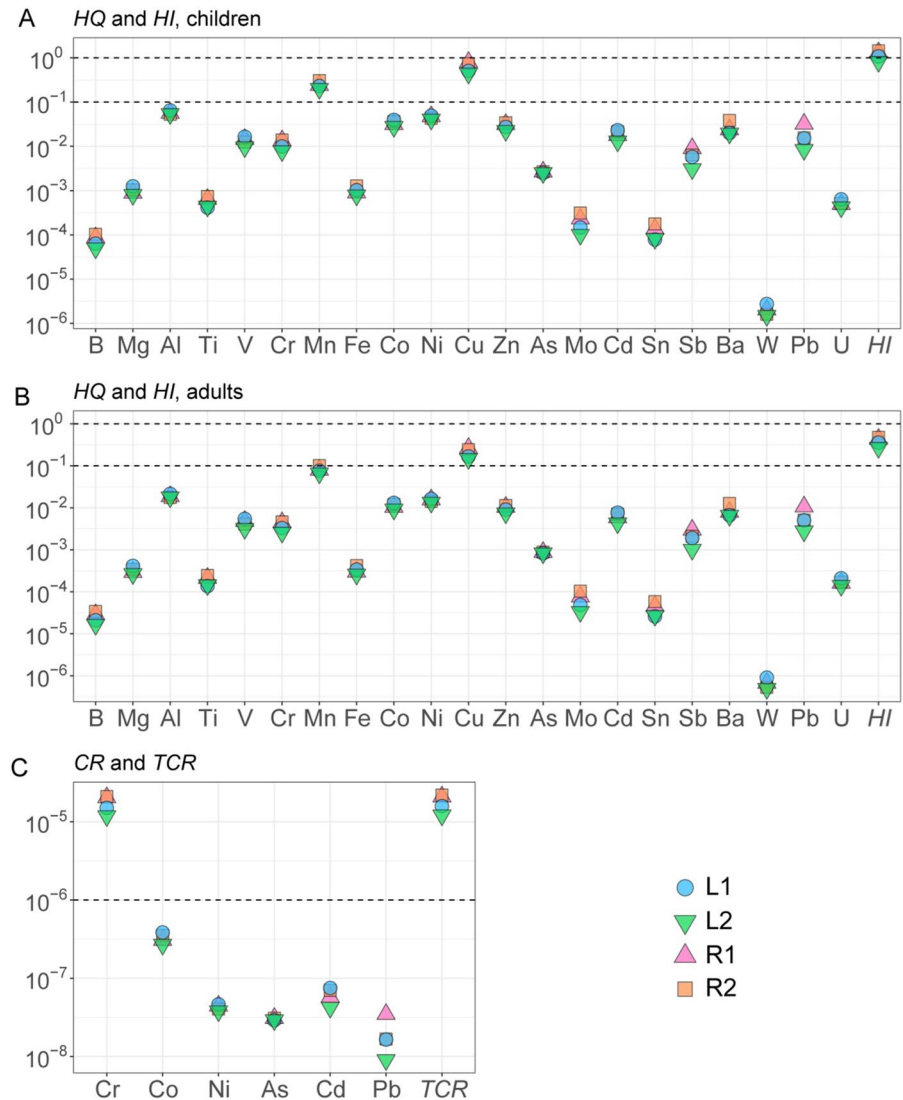
In general, during the lockdown period L in Moscow, the contribution of urban dust was significant for Bi (72%), Sn, Zr, Cr, Cu (45–54%), Fe, Mo, Sb, Zn, and Ca (25–30%); combustion and exhaust traffic emissions strongly influence the concentrations of Cs, V, B, Cd, Sb, and K (20–41%); the contribution of industrial emissions was significant for Ni, Mo, Ti, Cd (52–70%), W, Zr, Pb, Co, and V (24–42%); non-exhaust traffic emissions contributed a lot to Sb, Cu, Pb, and Cd (11–23%); the proportion of deicing salts was substantial for Na (90%), S, Zn, W, Ca, K, Co (45–54%), Pb, Cu, B, Fe, and Cr (29–45%) (Fig. 6).

Throughout the recovery period R after the removal of restrictions compared to the lockdown period L, lower contribution of industrial sources to PTEs, especially Mo, Cd, Ti, Zr, Pb, Ni, V, Cr, Co, and Fe (by 10%–28%), was noted (Fig. 6). This may be attributed to the end of the heating season and the rise in contributions from other sources. Thus, the contribution of urban dust to PTEs increased by 15%–26% for Mo, Ti, Cr, Fe, Zn, Ca, Zr, Co, Sn, and K, combustion and exhaust traffic emissions by 5%–8% for V, Cd, Pb, K, and S, and non-exhaust traffic emissions by 5%–15% for Pb, Cd, Sb, S, and Cu. This can be explained by the increase of anthropogenic activities following the removal of restrictions, which aligns with the data indicating an increase in urban dust blowing in summer as a result of rapid drying of roadways and topsoils after rains (Gubanova et al., 2022). On the other hand, the contribution of deicing salts to PTEs, especially Zn, Cu, S, Ca, K, B, Fe, Co, Cr, Sn, Pb, and Cs, also decreased by 10%–20%, resulting from the lower input of deicing agents from soil and road surfaces in summer due to their gradual washing out by rains.

Health risk assessment

In order to evaluate the impact of restrictive measures on the air pollution hazard posed by PTEs, non-carcinogenic and carcinogenic risks were calculated, and the corresponding results for the four studied periods (L1, L2, R1, R2) are depicted in Fig. 7. Non-carcinogenic risk decreases in the following sequence:

Fig. 7 The non-carcinogenic risks HQ for selected PTEs and the total non-carcinogenic risk HI for **A** children and **B** adults; **C** carcinogenic risks CR for selected PTEs and the total carcinogenic risk TCR during and after the lockdown



Cu > Mn > Al > Ni > Co > Ba > Zn > Cd > Pb > V > Cr > Sb > As > Fe > Mg > Ti > U > Mo > Sn > B > W. At the same time, in terms of non-carcinogenic risk hazard quotient (HQ), only Cu and Mn for children and Cu for adults fall into the gradation of low hazard (0.1–1). The remaining elements are characterized by $HQ < 0.1$, thus indicating no health risk during all studied periods. The median level of total non-carcinogenic risk HI for children is moderate (1.08–1.44) during the first period of restrictions L1 and after the removal of restrictions (R1 and R2) and decreases to the low hazard ($HI = 0.82$) during the second period of lockdown L2. Throughout all periods, the median value of HI for adults corresponds to the low hazard

level (0.27–0.47). In general, the non-carcinogenic risk HI for children is three times higher than for adults. The lowest levels of HQ for all PTEs are typical for the second period of the lockdown L2. The highest levels for B, Ti, Cr, Mn, Fe, Cu, Zn, As, Mo, Sn, Sb, Ba, and Pb were observed after the removal of restrictions during R1 and R2, and for Mg, Al, V, Co, Ni, Cd, W, and U during the first period L1.

The carcinogenic risk CR decreases in the following sequence of elements: Cr > Co > Cd > Ni > As > Pb. Chromium provides a low carcinogenic risk from 1.19×10^{-5} to 2.10×10^{-5} ; other PTEs are characterized by very low CR , not exceeding a threshold value of 10^{-6} . The total carcinogenic risk TCR remains at a

low level throughout all the studied periods (median *TCR* ranges from 1.21×10^{-5} to 2.20×10^{-5}), primarily driven by the presence of Cr. The lowest levels of *CR* for all PTEs, as well as *TCR* are characteristic of the lockdown period L2; the highest levels for Co, Ni, and Cd are typical of L1, and for Cr, As, and Pb during R1 and R2.

In the period of restrictions, the median levels of total non-carcinogenic and carcinogenic risks decreased by 24% and 23%, respectively, from a moderate hazard in L1 to low one in L2 for non-carcinogenic risk and remaining at the level of low risk for the carcinogenic risk (Fig. 8). After the lockdown, the risks increase by 61% and 72%, respectively, with non-carcinogenic risk returning from the low hazard in L2 to moderate hazard in R1. However, the median levels of the total non-carcinogenic and carcinogenic risks continue to grow and increase from R1 to R2 by 10% and 5%, respectively. The increase in risks under regular economic and industrial activities poses a persistent danger to the city’s population.

The non-carcinogenic and carcinogenic risks represent the first assessment of such a hazard from PM₁₀-bound PTEs for the population of Moscow. However, these results should be used with caution as the 3-month averaging period is too short to provide accurate estimates over a longer period and does not account for seasonal variations in air pollution. Although analyzing the impact of restrictive measures on changing risks to the population from PTE-polluted air and other urban environments is a

relatively common practice (Chakraborty et al., 2022; Lara et al., 2021; Lee et al., 2022; Martínez Morales et al., 2023; Selvam et al., 2022; Wang et al., 2022), such estimates often assume that the time of exposure of the population to pollutants is equivalent to the duration of the lockdown. However, the lockdown implies a significant reduction in human presence on the streets, resulting in a sharp decrease in the exposure time to outdoor air. Consequently, there is a substantial increase in the exposure time to indoor air. In addition, when calculating carcinogenic risk, exposure is averaged over 70 years, while the lockdown period lasted only a few months, so in general, such a short period of reduction in air pollution should not significantly affect an individual’s risk of cancer. Despite the existing limitations, such calculations during and after the lockdown are necessary to assess the reduction of risks for the urban population with a decrease in anthropogenic activity in the city, which is useful when planning measures to limit traffic and industrial emissions, as well as to clean roads from dust.

Conclusions

A first attempt was made to analyze changes in the concentrations of atmospheric PM₁₀-bound PTEs in the urban background of Moscow during and after the removal of COVID-19 restrictions, which took place from April 24 to June 30, 2020. It was observed

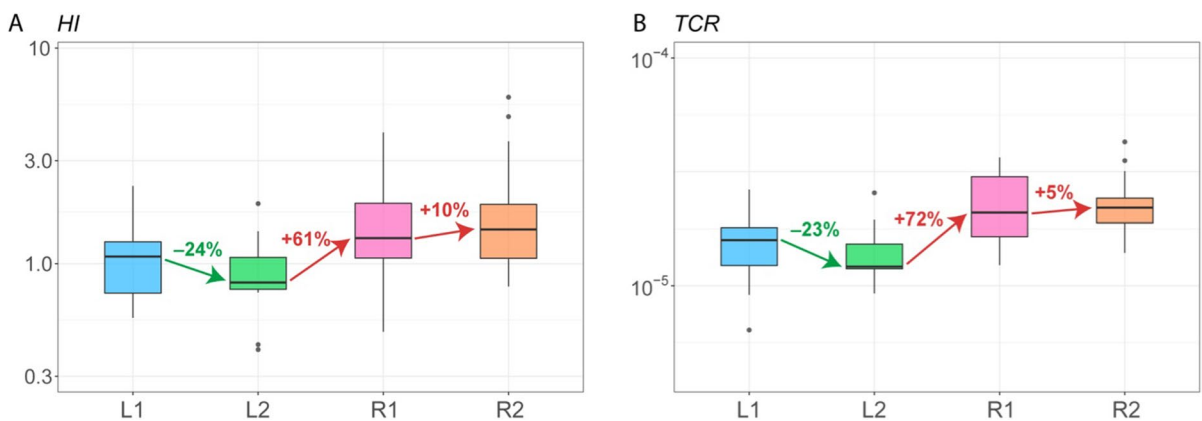


Fig. 8 Changes in median **A** total non-carcinogenic risks *HI* for children, and **B** total carcinogenic risks *TCR* of PM₁₀-bound PTEs during and after the lockdown. *HI* values

for adults are not shown since the patterns of their change completely repeat the *HI* changes for children

that there were significant changes in the elemental composition of PM₁₀ during these periods. During the lockdown, the concentrations of most PTEs from anthropogenic sources decreased by 10%–50%, and the total enrichment of PM₁₀ with PTEs also decreased by 38%. Rains reduced the input of PTEs from natural sources. After the removal of restrictions, air pollution with PTEs recovered, resulting in 152% increase in the total enrichment of PM₁₀, mainly due to growing contributions of urban dust (up to 26% increase), non-exhaust traffic emissions (up to 15%), combustion and exhaust traffic emissions (up to 8%), and simultaneously decreasing contributions of industrial sources (up to 28%) and deicing salts (up to 20%). However, the anomalous amount of precipitation in late May and the first half of June led to a relatively extended 2-week period of air pollution recovery. Throughout all the periods under investigation, the leading pollutants with a high enrichment of PM₁₀ particles were Sb, Cd, Sn, Bi, S, Pb, Cu, Mo, and Zn. Their anomalies are also typical for other components of the Moscow environment, thus indicating the presence of intense sources of these PTEs in the city. The non-carcinogenic and carcinogenic risks calculated for the population of Moscow are a first assessment of such a hazard from atmospheric PM₁₀-bound PTEs. These risks increased significantly after the lockdown, creating an increased danger under regular economic and industrial activities. The results of the real-time experiment during the lockdown could help plan measures to reduce the anthropogenic load from certain groups of sources in order to improve the quality of urban air.

Acknowledgements The authors are grateful to R.G. Kovach for the development of sampling and data treatment methods, and G.L. Shinkareva for the language editing services. Research was carried out with the equipment of MSU Shared Research Equipment Center “Technologies for obtaining new nanostructured materials and their complex study” and National Project “Science”.

Authors' contributions ADS was involved in formal analysis, investigation, writing—original draft, writing—review & editing, and visualization. DVV participated in conceptualization, investigation, methodology, software, formal analysis, writing—original draft, writing—review & editing, and visualization. OBP took part in sampling, investigation, data curation, resources, writing—review & editing, supervision, and funding acquisition. NEK was involved in conceptualization, methodology, data curation, writing—review & editing, supervision, project administration, and funding acquisition. MAC

participated in resources, writing—review & editing. NSK was involved in conceptualization, methodology, writing—review & editing, supervision, and funding acquisition.

Funding A sampling of PM₁₀ for further chemical analysis was carried out within the project of the Russian Geographical Society (contract No. 08/07-2020-Mo). The study of the enrichment of PM₁₀ with PTEs was financially supported by the Russian Science Foundation (Project No. 19-77-30004-II). Source apportionment of PM₁₀-bound PTEs was financially supported by the grant of the Ministry of Science and Higher Education of the Russian Federation (Project No. 075-15-2021-574). The funding sources had no involvement in the research and preparation of the article, in study design, collection, analysis, and interpretation of data, in writing the paper, and in the decision to submit the article for publication.

Data availability Data are available within the article and its supplementary materials. Additional data are available on request from the corresponding author.

Declarations

Conflict of interests The authors declare that they have no known competing financial interests or personal relationships that could have appeared to influence the work reported in this paper.

References

- Ali, M. U., Liu, G., Yousaf, B., Ullah, H., Abbas, Q., & Munir, M. A. M. (2019). A systematic review on global pollution status of particulate matter-associated potential toxic elements and health perspectives in urban environment. *Environmental Geochemistry and Health*, 41(3), 1131–1162. <https://doi.org/10.1007/s10653-018-0203-z>
- Alves, C. A., Barbosa, C., Rocha, S., Calvo, A., Nunes, T., Cerqueira, M., et al. (2015). Elements and polycyclic aromatic hydrocarbons in exhaust particles emitted by light-duty vehicles. *Environmental Science and Pollution Research*, 22(15), 11526–11542. <https://doi.org/10.1007/s11356-015-4394-x>
- Alves, C. A., Evtuygina, M., Vicente, A. M. P., Vicente, E. D., Nunes, T. V., Silva, P. M. A., et al. (2018). Chemical profiling of PM₁₀ from urban road dust. *Science of the Total Environment*, 634, 41–51. <https://doi.org/10.1016/j.scitotenv.2018.03.338>
- Ashton, E. C., & Macintosh, D. J. (2002). Preliminary assessment of the plant diversity and community ecology of the Sematan mangrove forest, Sarawak, Malaysia. *Forest Ecology and Management*, 166(1–3), 111–129. [https://doi.org/10.1016/S0378-1127\(01\)00673-9](https://doi.org/10.1016/S0378-1127(01)00673-9)
- Bencharif-Madani, F., Ali-Khodja, H., Kemmouche, A., Terrouche, A., Lokorai, K., Naidja, L., & Bouziane, M. (2019). Mass concentrations, seasonal variations, chemical compositions and element sources of PM₁₀ at an urban site in Constantine, northeast Algeria. *Journal of Geochemical Exploration*, 206, 106356. <https://doi.org/10.1016/j.gexplo.2019.106356>

- Bitjukova, V. R., & Saulskaya, T. D. (2017). Changes of the anthropogenic impact of Moscow industrial zones during the recent decades. *Vestnik Moskovskogo Universtiteta, Seriya Geografiya*, 3, 24–33.
- Bozkurt, Z., Gaga, O. E., Taşpınar, F., Arı, A., Pekey, B., Pekey, H., et al. (2018). Atmospheric ambient trace element concentrations of PM₁₀ at urban and sub-urban sites: source apportionment and health risk estimation. *Environmental Monitoring and Assessment*, 190(3), 168. <https://doi.org/10.1007/s10661-018-6517-6>
- Cal EPA. (2022). *California Environmental Protection Agency*. <https://oehha.ca.gov>. Accessed 18 July, 2022.
- Chakraborty, B., Bera, B., Adhikary, P. P., Bhattacharjee, S., Roy, S., Saha, S., et al. (2022). Effects of COVID-19 lockdown and unlock on the health of tropical large river with associated human health risk. *Environmental Science and Pollution Research*, 29(24), 37041–37056. <https://doi.org/10.1007/s11356-021-17881-w>
- Chon, K., Kim, Y., Bae, D. H., & Cho, J. (2015). Confirming anthropogenic influences on the major organic and inorganic constituents of rainwater in an urban area. *Drinking Water Engineering and Science*, 8(2), 35–48. <https://doi.org/10.5194/dwes-8-35-2015>
- Christian, T. J., Yokelson, R. J., Cardenas, B., Molina, L. T., & Engling, G. (2010). Trace gas and particle emissions from domestic and industrial biofuel use and garbage burning in central Mexico. *Atmospheric Chemistry and Physics*, 10, 565–584. <https://doi.org/10.5194/acp-10-565-2010>
- Chubarova, N. E., Nezval', E. I., Belikov, I. B., Gorbarenko, E. V., Eremina, I. D., Zhdanova, E. Y., et al. (2014). Climatic and environmental characteristics of Moscow megalopolis according to the data of the Moscow State University Meteorological Observatory over 60 years. *Russian Meteorology and Hydrology*, 39(9), 602–613. <https://doi.org/10.3103/S1068373914090052>
- Chubarova, N. E., Androsova, Y. Y., & Lezina, Y. A. (2021). The dynamics of the atmospheric pollutants during the Covid-19 pandemic 2020 and their relationship with meteorological conditions in Moscow. *Geography, Environment, Sustainability*, 14(4), 168–182. <https://doi.org/10.24057/2071-9388-2021-012>
- Clemente, Á., Yubero, E., Nicolás, J. F., Caballero, S., Crespo, J., & Galindo, N. (2022). Changes in the concentration and composition of urban aerosols during the COVID-19 lockdown. *Environmental Research*, 203, 111788. <https://doi.org/10.1016/j.envres.2021.111788>
- Elansky, N. F., Ponomarev, N. A., & Verevkin, Y. M. (2018). Air quality and pollutant emissions in the Moscow megacity in 2005–2014. *Atmospheric Environment*, 175, 54–64. <https://doi.org/10.1016/j.atmosenv.2017.11.057>
- Elansky, N. F., Shilkin, A. V., Ponomarev, N. A., Semutnikova, E. G., & Zakharova, P. V. (2020). Weekly patterns and weekend effects of air pollution in the Moscow megacity. *Atmospheric Environment*, 224, 117303. <https://doi.org/10.1016/j.atmosenv.2020.117303>
- Erina, O., Tereshina, M., Shinkareva, G., Sokolov, D., & Lychagin, M. (2021). Natural background and transformation of water quality in the Moskva River. *IOP Conference Series: Earth and Environmental Science*, 834(1), 012055. <https://doi.org/10.1088/1755-1315/834/1/012055>
- Ermolin, M. S., Fedotov, P. S., Ivaneev, A. I., Karandashev, V. K., Fedyunina, N. N., & Burmistrov, A. A. (2018). A contribution of nanoscale particles of road-deposited sediments to the pollution of urban runoff by heavy metals. *Chemosphere*, 210, 65–75. <https://doi.org/10.1016/j.chemosphere.2018.06.150>
- Fang, B., Zeng, H., Zhang, L., Wang, H., Liu, J., Hao, K., et al. (2021). Toxic metals in outdoor/indoor airborne PM_{2.5} in port city of Northern, China: Characteristics, sources, and personal exposure risk assessment. *Environmental Pollution*, 279, 116937. <https://doi.org/10.1016/j.envpol.2021.116937>
- Fedotov, P. S., Ermolin, M. S., Karandashev, V. K., & Ladonin, D. V. (2014). Characterization of size, morphology and elemental composition of nano-, submicron, and micron particles of street dust separated using field-flow fractionation in a rotating coiled column. *Talanta*, 130, 1–7. <https://doi.org/10.1016/j.talanta.2014.06.040>
- Ghanbarian, M., Nicknam, M. H., Mesdaghinia, A., Yunesian, M., Hassanvand, M. S., Soleimanifar, N., et al. (2019). Investigation and comparison of in vitro genotoxic potency of PM₁₀ collected in rural and urban sites at Tehran in different metrological conditions and different seasons. *Biological Trace Element Research*, 189(1), 301–310. <https://doi.org/10.1007/s12011-018-1469-9>
- Ginzburg, A. S., Semenov, V. A., Semutnikova, E. G., Aleshina, M. A., Zakharova, P. V., & Lezina, E. A. (2020). Impact of COVID-19 lockdown on air quality in Moscow. *Doklady Earth Sciences*, 495(1), 862–866. <https://doi.org/10.1134/S1028334X20110069>
- Greenstone, M., & Fan, C. Q. (2018). *Introducing the air quality life index: Twelve facts about particulate air pollution, human health, and global policy*. Chicago. <https://aqli.epic.uchicago.edu/wp-content/uploads/2018/11/AQLI-Intro-Report.pdf>. Accessed 5 July, 2022.
- Grivas, G., Cheristanidis, S., Chaloulakou, A., Koutrakis, P., & Mihalopoulos, N. (2018). Elemental composition and source apportionment of fine and coarse particles at traffic and urban background locations in Athens, Greece. *Aerosol and Air Quality Research*, 18(7), 1642–1659. <https://doi.org/10.4209/aaqr.2017.12.0567>
- Gubanov, D. P., Iordanskii, M. A., Kuderina, T. M., Skorokhod, A. I., Elansky, N. F., & Minashkin, V. M. (2021a). Elemental composition of aerosols in the near-surface air of Moscow: Seasonal changes in 2019 and 2020. *Atmospheric and Oceanic Optics*, 34(5), 475–482. <https://doi.org/10.1134/S1024856021050122>
- Gubanov, D. P., Vinogradova, A. A., Iordanskii, M. A., & Skorokhod, A. I. (2021b). Time variations in the composition of atmospheric aerosol in Moscow in spring 2020. *Izvestiya, Atmospheric and Oceanic Physics*, 57(3), 297–309. <https://doi.org/10.1134/S0001433821030051>
- Gubanov, D. P., Vinogradova, A. A., Iordanskii, M. A., & Skorokhod, A. I. (2022). Variability of near-surface aerosol composition in Moscow in 2020–2021: Episodes of extreme air pollution of different genesis. *Atmosphere*, 13(4), 574. <https://doi.org/10.3390/atmos13040574>
- Guo, J., Kang, S., Huang, J., Zhang, Q., Tripathee, L., & Silanpää, M. (2015). Seasonal variations of trace elements

- in precipitation at the largest city in Tibet, Lhasa. *Atmospheric Research*, 153, 87–97. <https://doi.org/10.1016/j.atmosres.2014.07.030>
- Haji Gholizadeh, M., Melesse, A. M., & Reddi, L. (2016). Water quality assessment and apportionment of pollution sources using APCS-MLR and PMF receptor modeling techniques in three major rivers of South Florida. *Science of the Total Environment*, 566–567, 1552–1567. <https://doi.org/10.1016/j.scitotenv.2016.06.046>
- Hartwell, C. A., Otrachshenko, V., & Popova, O. (2021). Waxing power, waning pollution: The effect of COVID-19 on Russian environmental policymaking. *Ecological Economics*, 184, 107003. <https://doi.org/10.1016/j.ecolecon.2021.107003>
- He, C., Hong, S., Zhang, L., Mu, H., Xin, A., Zhou, Y., et al. (2021). Global, continental, and national variation in PM_{2.5}, O₃, and NO₂ concentrations during the early 2020 COVID-19 lockdown. *Atmospheric Pollution Research*, 12(3), 136–145. <https://doi.org/10.1016/j.apr.2021.02.002>
- Huang, C.-H., Ko, Y.-R., Lin, T.-C., Cheng, Y.-H., Chen, Y.-C., & Ting, Y.-C. (2023). Implications of the improvement in atmospheric fine particles: A case study of COVID-19 pandemic in Northern Taiwan. *Aerosol and Air Quality Research*, 23, 220329. <https://doi.org/10.4209/aaqr.220329>
- Hudda, N., Simon, M. C., Patton, A. P., & Durant, J. L. (2020). Reductions in traffic-related black carbon and ultrafine particle number concentrations in an urban neighborhood during the COVID-19 pandemic. *Science of the Total Environment*, 742, 140931. <https://doi.org/10.1016/j.scitotenv.2020.140931>
- Hwang, H.-M., Fiala, M. J., Park, D., & Wade, T. L. (2016). Review of pollutants in urban road dust and stormwater runoff: Part 1. Heavy metals released from vehicles. *International Journal of Urban Sciences*, 20(3), 334–360. <https://doi.org/10.1080/12265934.2016.1193041>
- Ivaneev, A. I., Brzhezinskiy, A. S., Karandashev, V. K., Ermolin, M. S., & Fedotov, P. S. (2023). Assessment of sources, environmental, ecological, and health risks of potentially toxic elements in urban dust of Moscow megacity, Russia. *Chemosphere*, 321, 138142. <https://doi.org/10.1016/j.chemosphere.2023.138142>
- Jia, C., Li, W., Wu, T., & He, M. (2021). Road traffic and air pollution: Evidence from a nationwide traffic control during coronavirus disease 2019 outbreak. *Science of the Total Environment*, 781, 146618. <https://doi.org/10.1016/j.scitotenv.2021.146618>
- Kabata-Pendias, A. (2011). *Trace elements in soils and plants* (4th ed.). CRC Press.
- Kasimov, N. S., Kosheleva, N. E., Vlasov, D. V., Nabelkina, K. S., & Ryzhov, A. V. (2019). Physicochemical properties of road dust in Moscow. *Geography, Environment, Sustainability*, 12(4), 96–113. <https://doi.org/10.24057/2071-9388-2019-55>
- Kasimov, N. S., Vlasov, D. V., & Kosheleva, N. E. (2020). Enrichment of road dust particles and adjacent environments with metals and metalloids in eastern Moscow. *Urban Climate*, 32, 100638. <https://doi.org/10.1016/j.uclim.2020.100638>
- Kirilina, N. A. (2020). Changes of traffic mobility and road traffic injuries in Moscow during lockdown. *Revista Inclusiones*, 7, 285–308.
- Kosheleva, N. E., Vlasov, D. V., Korlyakov, I. D., & Kasimov, N. S. (2018). Contamination of urban soils with heavy metals in Moscow as affected by building development. *Science of the Total Environment*, 636, 854–863. <https://doi.org/10.1016/j.scitotenv.2018.04.308>
- Kul'bachevskii, A. O. (2020). *Report on the State of the Environment in Moscow in 2019*. Department of Nature Management and Environmental Protection of Moscow Government. <https://www.mos.ru/eco/documents/doklady/view/240948220/>. Accessed 28 July, 2020.
- Kul'bachevskii, A. O. (2021). *Report on the State of the Environment in Moscow in 2020*. Department of Nature Management and Environmental Protection of Moscow Government. <https://www.mos.ru/eco/documents/doklady/view/259642220/>. Accessed April 10, 2022.
- Ladonin, D. V., & Mikhaylova, A. P. (2020). Heavy metals and arsenic in soils and street dust of the Southeastern Administrative District of Moscow: Long-term data. *Eurasian Soil Science*, 53(11), 1635–1644. <https://doi.org/10.1134/S1064229320110095>
- Landing, W. M., Caffrey, J. M., Nolek, S. D., Gosnell, K. J., & Parker, W. C. (2010). Atmospheric wet deposition of mercury and other trace elements in Pensacola, Florida. *Atmospheric Chemistry and Physics*, 10(10), 4867–4877. <https://doi.org/10.5194/acp-10-4867-2010>
- Lara, R., Suárez-Peña, B., Megido, L., Negral, L., Rodríguez-Iglesias, J., Fernández-Nava, Y., & Castrillón, L. (2021). Health risk assessment of potentially toxic elements in the dry deposition fraction of settleable particulate matter in urban and suburban locations in the city of Gijón, Spain. *Journal of Environmental Chemical Engineering*, 9(6), 106794. <https://doi.org/10.1016/j.jece.2021.106794>
- Lara, R., Megido, L., Suárez-Peña, B., Negral, L., Fernández-Nava, Y., Rodríguez-Iglesias, J., et al. (2023). Impact of COVID-19 restrictions on hourly levels of PM₁₀, PM_{2.5} and black carbon at an industrial suburban site in northern Spain. *Atmospheric Environment*. <https://doi.org/10.1016/j.atmosenv.2023.119781>
- Lee, Y. S., Kim, Y. K., Choi, E., Jo, H., Hyun, H., Yi, S.-M., & Kim, J. Y. (2022). Health risk assessment and source apportionment of PM_{2.5}-bound toxic elements in the industrial city of Siheung, Korea. *Environmental Science and Pollution Research*. <https://doi.org/10.1007/s11356-022-20462-0>
- Lemly, A. D. (1996). Evaluation of the hazard quotient method for risk assessment of selenium. *Ecotoxicology and Environmental Safety*, 35(2), 156–162. <https://doi.org/10.1006/eesa.1996.0095>
- Li, R., Zhao, Y., Fu, H., Chen, J., Peng, M., & Wang, C. (2021). Substantial changes in gaseous pollutants and chemical compositions in fine particles in the North China Plain during the COVID-19 lockdown period: anthropogenic vs. meteorological influences. *Atmospheric Chemistry and Physics*, 21(11), 8677–8692. <https://doi.org/10.5194/acp-21-8677-2021>
- Liu, L., Lin, Q., Liang, Z., Du, R., Zhang, G., Zhu, Y., et al. (2021). Variations in concentration and solubility of iron in atmospheric fine particles during the COVID-19

- pandemic: An example from China. *Gondwana Research*, 97, 138–144. <https://doi.org/10.1016/j.gr.2021.05.022>
- Ma, Y., Mummullage, S., Wijesiri, B., Egodawatta, P., McGree, J., Ayoko, G. A., & Goonetilleke, A. (2021). Source quantification and risk assessment as a foundation for risk management of metals in urban road deposited solids. *Journal of Hazardous Materials*, 408, 124912. <https://doi.org/10.1016/j.jhazmat.2020.124912>
- Manchanda, C., Kumar, M., Singh, V., Faisal, M., Hazarika, N., Shukla, A., et al. (2021). Variation in chemical composition and sources of PM_{2.5} during the COVID-19 lockdown in Delhi. *Environment International*, 153, 106. <https://doi.org/10.1016/j.envint.2021.106541>
- Martínez Morales, S., Cerón Bretón, J. G., Carbajal, N., Cerón Bretón, R. M., Lara Severino, R., Kahl, J. D. W., et al. (2023). PM_{2.5}-bound trace metals in an urban area of Northern Mexico during the COVID-19 pandemic: Characterization, sources, and health risk. *Air Quality, Atmosphere & Health*. <https://doi.org/10.1007/s11869-023-01372-7>
- Massimi, L., Simonetti, G., Buiarelli, F., Di Filippo, P., Pomata, D., Riccardi, C., et al. (2020). Spatial distribution of levoglucosan and alternative biomass burning tracers in atmospheric aerosols, in an urban and industrial hot-spot of Central Italy. *Atmospheric Research*, 239, 104904. <https://doi.org/10.1016/j.atmosres.2020.104904>
- Measures against coronavirus in Moscow. (2020). *Official website of the Mayor of Moscow*. <https://www.mos.ru/city/projects/measures>. Accessed January 25, 2021.
- Millán-Martínez, M., Sánchez-Rodas, D., Sánchez de la Campa, A. M., & de la Rosa, J. (2022). Impact of the SARS-CoV-2 lockdown measures in Southern Spain on PM₁₀ trace element and gaseous pollutant concentrations. *Chemosphere*, 303, 134853. <https://doi.org/10.1016/j.chemosphere.2022.134853>
- Nguyen, T. P. M., Bui, T. H., Nguyen, M. K., Nguyen, T. H., Vu, V. T., & Pham, H. L. (2021). Impact of Covid-19 partial lockdown on PM_{2.5}, SO₂, NO₂, O₃, and trace elements in PM_{2.5} in Hanoi, Vietnam. *Environmental Science and Pollution Research*. <https://doi.org/10.1007/s11356-021-13792-y>
- Nikiforova, E. M., Kasimov, N. S., & Kosheleva, N. E. (2014). Long-term dynamics of the anthropogenic salinization of soils in Moscow (by the example of the Eastern district). *Eurasian Soil Science*, 47(3), 203–215. <https://doi.org/10.1134/S1064229314030041>
- Ozaki, H., Yoshimura, K., Asaoka, Y., & Hayashi, S. (2021). Antimony from brake dust to the combined sewer collection system via road effluent under rainy conditions. *Environmental Monitoring and Assessment*, 193(6), 369. <https://doi.org/10.1007/s10661-021-09152-5>
- Pant, P., & Harrison, R. M. (2013). Estimation of the contribution of road traffic emissions to particulate matter concentrations from field measurements: A review. *Atmospheric Environment*, 77, 78–97. <https://doi.org/10.1016/j.atmosenv.2013.04.028>
- Pinto, U., & Maheshwari, B. L. (2011). River health assessment in peri-urban landscapes: An application of multivariate analysis to identify the key variables. *Water Research*, 45(13), 3915–3924. <https://doi.org/10.1016/j.watres.2011.04.044>
- Popovicheva, O., Chichaeva, M., Kovach, R., Zhdanova, E., & Kasimov N. (2022). Seasonal weekly and diurnal black carbon in Moscow megacity background under impact of urban and regional sources. *Atmosphere*, 13(4), 563. <https://doi.org/10.3390/atmos13040563>
- Pourret, O., & Hursthouse, A. (2019). It's time to replace the term “heavy metals” with “potentially toxic elements” when reporting environmental research. *International Journal of Environmental Research and Public Health*, 16(22), 4446. <https://doi.org/10.3390/ijerph16224446>
- Qiu, W., He, H., Xu, T., Jia, C., & Li, W. (2021). The air quality changes and related mortality benefits during the coronavirus disease 2019 pandemic in China: Results from a nationwide forecasting study. *Journal of Cleaner Production*, 308, 127327. <https://doi.org/10.1016/j.jclepro.2021.127327>
- Querol, X., Massagué, J., Alastuey, A., Moreno, T., Gangoiti, G., Mantilla, E., et al. (2021). Lessons from the COVID-19 air pollution decrease in Spain: Now what? *Science of the Total Environment*, 779, 146380. <https://doi.org/10.1016/j.scitotenv.2021.146380>
- Rakhmanin, Y. A., Novikov, S. M., Shashina, T. A., Ivanov, S. I., Avaliani, S. L., Bushtueva, K. A., et al. (2004). R 2.1.10.1920-04. *Human health risk Assessment from environmental chemicals*. Federal Center for State Sanitary and Epidemiological Supervision of the Ministry of Health of Russia.
- Ramírez, O., Sánchez de la Campa, A. M., Amato, F., Moreno, T., Silva, L. F., & de la Rosa, J. D. (2019). Physicochemical characterization and sources of the thoracic fraction of road dust in a Latin American megacity. *Science of the Total Environment*, 652, 434–446. <https://doi.org/10.1016/j.scitotenv.2018.10.214>
- Romzaykina, O. N., Vasenev, V. I., Paltseva, A., Kuzyakov, Y. V., Neaman, A., & Dovletyarova, E. A. (2021). Assessing and mapping urban soils as geochemical barriers for contamination by heavy metal(oid)s in Moscow megapolis. *Journal of Environmental Quality*, 50, 22–37. <https://doi.org/10.1002/jeq2.20142>
- Rudke, A. P., Martins, J. A., de Almeida, D. S., Martins, L. D., Beal, A., Hallak, R., et al. (2021). How mobility restrictions policy and atmospheric conditions impacted air quality in the State of São Paulo during the COVID-19 outbreak. *Environmental Research*, 198, 111255. <https://doi.org/10.1016/j.envres.2021.111255>
- Rudnick, R. L., & Gao, S. (2014). Composition of the continental crust. In *Treatise on geochemistry* (pp. 1–51). Elsevier. <https://doi.org/10.1016/B978-0-08-095975-7.00301-6>
- Russian Federal State Statistics Service. (2020). Length of public roads in the subjects of the Russian Federation. *Russian Federal State Statistics Service*. <https://rosstat.gov.ru/storage/mediabank/iNEf3mAv/t2-2.xls>. Accessed November 17, 2022.
- Selvam, S., Jesuraja, K., Roy, P. D., Venkatramanan, S., Khan, R., Shukla, S., et al. (2022). Human health risk assessment of heavy metal and pathogenic contamination in surface water of the Punnakayal estuary, South India.

- Chemosphere*, 298, 134027. <https://doi.org/10.1016/j.chemosphere.2022.134027>
- Shafer, M. M., Toner, B. M., Overdier, J. T., Schauer, J. J., Fakra, S. C., Hu, S., et al. (2012). Chemical speciation of vanadium in particulate matter emitted from diesel vehicles and urban atmospheric aerosols. *Environmental Science & Technology*, 46(1), 189–195. <https://doi.org/10.1021/es200463c>
- Shinkareva, G., Erina, O., Tereshina, M., Sokolov, D., Lychagin, M., & Kasimov, N. (2022). Anthropogenic factors affecting the Moskva River water quality: Levels and sources of nutrients and potentially toxic elements in Moscow metropolitan area. *Environmental Geochemistry and Health*. <https://doi.org/10.1007/s10653-022-01393-8>
- Sokhi, R. S., Singh, V., Querol, X., Finardi, S., Targino, A. C., de Andrade, M. F., et al. (2021). A global observational analysis to understand changes in air quality during exceptionally low anthropogenic emission conditions. *Environment International*, 157, 106818. <https://doi.org/10.1016/j.envint.2021.106818>
- Song, Y., Xie, S., Zhang, Y., Zeng, L., Salmon, L. G., & Zheng, M. (2006). Source apportionment of PM_{2.5} in Beijing using principal component analysis/absolute principal component scores and UNMIX. *Science of the Total Environment*, 372(1), 278–286. <https://doi.org/10.1016/j.scitotenv.2006.08.041>
- Thurston, G. D., & Spengler, J. D. (1985). A quantitative assessment of source contributions to inhalable particulate matter pollution in metropolitan Boston. *Atmospheric Environment* (1967), 19(1), 9–25. [https://doi.org/10.1016/0004-6981\(85\)90132-5](https://doi.org/10.1016/0004-6981(85)90132-5)
- TomTom Traffic Index. (2020). *tomtom.com*. https://www.tomtom.com/en_gb/traffic-index/ranking/. Accessed December 31, 2020.
- U.S. Borax. (2023). Boron in industrial fluids and lubricants. *U.S. Borax*. <https://www.borax.com/applications/industrial-fluids-lubricants>. Accessed May 29, 2023.
- U.S. EPA. (2011). *Exposure factors handbook: 2011 edition*. National Center for Environmental Assessment, Washington, DC; EPA/600/R-09/052F. Springfield: U.S. EPA.
- U.S. EPA. (2013). *Users' guide and background technical document for USEPA regions 9'S preliminary remediation goals*. Washington, D.C., USA: National Center for Environmental assessment. <https://semspub.epa.gov/work/02/103453.pdf>. Accessed May 29, 2023.
- U.S. EPA. (2014). *U. S. EPA. OSWER Directive 9200.1-120. Human health evaluation manual, supplemental guidance: Update to standard default exposure factors*. Washington, DC: National Center for Environmental assessment. <https://www.epa.gov/risk/oswer-directive-92001-120>. Accessed May 29, 2023.
- U.S. EPA. (2022). Regional Screening Levels (RSLs)—Generic Tables. May, 2022. <https://www.epa.gov/risk/regional-screening-levels-rsls-generic-tables>. Accessed July 8, 2022.
- Van Den Heuvel, R., Den Hond, E., Govarts, E., Colles, A., Koppen, G., Staelens, J., et al. (2016). Identification of PM₁₀ characteristics involved in cellular responses in human bronchial epithelial cells (Beas-2B). *Environmental Research*, 149, 48–56. <https://doi.org/10.1016/j.envres.2016.04.029>
- Varol, M. (2011). Assessment of heavy metal contamination in sediments of the Tigris River (Turkey) using pollution indices and multivariate statistical techniques. *Journal of Hazardous Materials*, 195, 355–364. <https://doi.org/10.1016/j.jhazmat.2011.08.051>
- Vergel, K., Zinicovscaia, I., Yushin, N., Chaligava, O., Nekhoroshkov, P., & Grozdov, D. (2022). Moss biomonitoring of atmospheric pollution with trace elements in the Moscow region, Russia. *Toxics*, 10(2), 66. <https://doi.org/10.3390/toxics10020066>
- Vinokurov, S. F., Tarasova, N. P., Trunova, A. N., & Sychkova, V. A. (2017). A comprehensive analysis of the content of heavy rare-earth elements and platinum in snow samples to assess the ecological hazard of air pollution in urban areas. *Doklady Earth Sciences*, 475(1), 771–774. <https://doi.org/10.1134/S1028334X17070108>
- Vlasov, D. V., Shinkareva, G. L., & Kasimov, N. S. (2019). Metals and metalloids in bottom sediments of lakes and ponds of the eastern part of Moscow. *Vestnik Moskovskogo Universiteta, Seriya Geografiya*, 4(4), 43–52.
- Vlasov, D. V., Vasil'chuk, J., Kosheleva, N., & Kasimov, N. (2020). Dissolved and suspended forms of metals and metalloids in snow cover of megacity: Partitioning and deposition rates in Western Moscow. *Atmosphere*, 11, 907. <https://doi.org/10.3390/atmos11090907>
- Vlasov, D. V., Kasimov, N., Eremina, I., Shinkareva, G., & Chubarova, N. (2021a). Partitioning and solubilities of metals and metalloids in spring rains in Moscow megacity. *Atmospheric Pollution Research*, 12(1), 255–271. <https://doi.org/10.1016/j.apr.2020.09.012>
- Vlasov, D. V., Kosheleva, N., & Kasimov, N. (2021b). Spatial distribution and sources of potentially toxic elements in road dust and its PM₁₀ fraction of Moscow megacity. *Science of the Total Environment*, 761, 143267. <https://doi.org/10.1016/j.scitotenv.2020.143267>
- Vlasov, D. V., Kukushkina, O. V., Kosheleva, N. E., & Kasimov, N. S. (2022). Levels and factors of the accumulation of metals and metalloids in roadside soils, road dust and their PM₁₀ fraction in the Western Okrug of Moscow. *Eurasian Soil Science*, 55(5), 556–572. <https://doi.org/10.1134/S1064229322050118>
- Vlasov, D. V., Kasimov, N., Eremina, I., Shinkareva, G., & Chubarova, N. (2023a). Major ions and potentially toxic elements in atmospheric precipitation during the COVID-19 lockdown in Moscow megacity. *Urban Climate*, 48, 101422. <https://doi.org/10.1016/j.uclim.2023.101422>
- Vlasov, D. V., Vasil'chuk, J. Y., Kosheleva, N. E., & Kasimov, N. S. (2023b). Contamination levels and source apportionment of potentially toxic elements in size-fractionated road dust of Moscow. *Environmental Science and Pollution Research*, 30(13), 38099–38120. <https://doi.org/10.1007/s11356-022-24934-1>
- Voronov, A., Mishina, V., & Buranov, I. (2019, March 23). Moscow lightly salted. "The Kommersant" newspaper. <https://www.kommersant.ru/doc/3922297>. Accessed April 10, 2022.
- Wang, G., Huang, K., Fu, Q., Chen, J., Huo, J., Zhao, Q., et al. (2022). Response of PM_{2.5}-bound elemental species to emission variations and associated health risk assessment during the COVID-19 pandemic in a coastal

- megacity. *Journal of Environmental Sciences*, 122, 115–127. <https://doi.org/10.1016/j.jes.2021.10.005>
- Wang, H., Miao, Q., Shen, L., Yang, Q., Wu, Y., & Wei, H. (2021a). Air pollutant variations in Suzhou during the 2019 novel coronavirus (COVID-19) lockdown of 2020: High time-resolution measurements of aerosol chemical compositions and source apportionment. *Environmental Pollution*, 271, 116298. <https://doi.org/10.1016/j.envpol.2020.116298>
- Wang, S., Yan, Y., Yu, R., Shen, H., Hu, G., & Wang, S. (2021b). Influence of pollution reduction interventions on atmospheric PM_{2.5}: A case study from the 2017 Xiamen. *Atmospheric Pollution Research*, 12(8), 101137. <https://doi.org/10.1016/j.apr.2021.101137>
- Wang, Y., Liu, B., Zhang, Y., Dai, Q., Song, C., Duan, L., et al. (2021c). Potential health risks of inhaled toxic elements and risk sources during different COVID-19 lockdown stages in Linfen, China. *Environmental Pollution*, 284, 117454. <https://doi.org/10.1016/j.envpol.2021.117454>
- Wang, Y., Wen, Y., Cui, Y., Guo, L., He, Q., Li, H., & Wang, X. (2021d). Substantial changes of chemical composition and sources of fine particles during the period of COVID-19 pandemic in Taiyuan, Northern China. *Air Quality, Atmosphere & Health*. <https://doi.org/10.1007/s11869-021-01082-y>
- WHO. (2013). *Review of evidence on health aspects of air pollution—REVIHAAP Project Technical Report*. World Health Organization. https://www.euro.who.int/__data/assets/pdf_file/0004/193108/REVIHAAP-Final-technical-report-final-version.pdf. Accessed July 5, 2022.
- Yandex. (2021). *Self-isolation index*. <https://yandex.ru/company/researches/2020/podomam>. Accessed July 31, 2021.
- Zappi, A., Popovicheva, O., Tositti, L., Chichaeva, M., Eremina, I., Kasper-Giebl, A., et al. (2023). Factors influencing aerosol and precipitation ion chemistry in urban background of Moscow megacity. *Atmospheric Environment*, 294, 119458. <https://doi.org/10.1016/j.atmosenv.2022.119458>

Publisher's Note Springer Nature remains neutral with regard to jurisdictional claims in published maps and institutional affiliations.

Springer Nature or its licensor (e.g. a society or other partner) holds exclusive rights to this article under a publishing agreement with the author(s) or other rightsholder(s); author self-archiving of the accepted manuscript version of this article is solely governed by the terms of such publishing agreement and applicable law.